Modeling of the interactions between forest vegetation, disturbances, and sediment yields

Erkan Istanbulluoglu,[1] David G. Tarboton, and Robert T. Pack

Civil and Environmental Engineering Department, Utah State University, Logan, Utah, USA

Charles H. Luce

Rocky Mountain Research Station, U.S. Forest Service, Boise, Idaho, USA

[1] The controls of forest vegetation, wildfires, and harvest vegetation disturbances on the frequency and magnitude of sediment delivery from a small watershed ($\sim$3.9 km^2) in the Idaho batholith are investigated through numerical modeling. The model simulates soil development based on continuous bedrock weathering and the divergence of diffusive sediment transport on hillslopes. Soil removal is due to episodic gully erosion, shallow landsliding, and debris flow generation. In the model, forest vegetation provides root cohesion and surface resistance to channel initiation. Forest fires and harvests reduce the vegetation. Vegetation loss leaves the land susceptible to erosion and landsliding until the vegetation cover reestablishes in time. Simulation results compare well with field observations of event sediment yields and long-term averages over $\sim$10,000 years. When vegetation is not disturbed by wildfires over thousands of years, sediment delivery is modeled to be less frequent but with larger event magnitudes. Increased values of root cohesion (representing denser forests) lead to higher event magnitudes. Wildfires appear to control the timing of sediment delivery. Compared to undisturbed forests, erosion is concentrated during the periods with low erosion thresholds, often called accelerated erosion periods, following wildfires. Our modeling suggests that drainage density is inversely proportional to root cohesion and that reduced forest cover due to wildfires increases the drainage density. We compare the sediment yields under anthropogenic (harvest) and natural (wildfire) disturbances. Disturbances due to forest harvesting appear to increase the frequency of sediment delivery; however, the sediment delivery following wildfires seems to be more severe. These modeling-based findings have implications for engineering design and environmental management, where sediment inputs to streams and the fluctuations and episodicity of these inputs are of concern.   INDEX TERMS: 1625 Global Change: Geomorphology and weathering (1824, 1886); 1815 Hydrology: Erosion and sedimentation; 1824 Hydrology: Geomorphology (1625); *KEYWORDS:* sediment yield, wildfires, forest management, hydrology

1. Introduction

[2] Episodic debris flows and gully erosion are the major geomorphic processes involved in the development of steep mountainous regions in tectonically active humid environments [*Selby*, 1993]. Episodic erosion delivers a punctuated sediment supply to channels that may cause property damage and loss of life [*Sidle et al.*, 1985; *Crozier*, 1986], kill fish, disturb aquatic habitats [*Pollok*, 1998; *Reeves et al.*, 1998], and cause silting in reservoirs that reduces their operational lifespan. Understanding the factors that control the natural rates of erosion and their variability and timing in mountainous basins is important for assessing the environmental risks associated with erosion events and for predicting the impacts of land use on erosion [*Dietrich et al.*, 2000; *Kirchner et al.*, 2001].

[3] It has been argued that in rivers, most of the sediment is carried by floods, which recur at least once in 5 years [*Wolman and Miller*, 1960]. The importance of extreme events in geomorphology on the scale of hillslopes, however, has been a neglected topic because of the lack of data and techniques to date past low-frequency and large-magnitude events [*Selby*, 1993]. *Kirchner et al.* [2001]

---

[1]Now at Department of Civil and Environmental Engineering, Massachusetts Institute of Technology, Cambridge, Massachusetts, USA.

compared long-term erosion rates over 10,000 year timescales with short-term measurements (10–84 years) in steep-forested Idaho watersheds and found that long-term average sediment yields are, on the average, 17 times higher than the short-term stream sediment fluxes. This significant difference suggests that sediment delivery from mountainous watersheds is extremely episodic and that long-term sediment delivery is dominated by catastrophic rare events [*Kirchner et al.*, 2001].

[4] In steep-forested basins of the western United States, catastrophic erosion events are often linked to extreme climate events together with vegetation disturbances by wildfires and anthropogenic activities such as timber removal [*Cannon et al.*, 2001; *Meyer et al.*, 2001]. These disturbances have shown to dramatically accelerate erosion rates over rates in undisturbed forests in short timescales [*Montgomery et al.*, 2000; *Megahan et al.*, 1978; *Sidle et al.*, 1985; *Gray and Megahan*, 1981]. Vegetation affects the geomorphic response of a basin directly by providing additional cohesion in the soil profile that tends to stabilize the land against landsliding and by enhancing thresholds for scour by overland flow [*Burroughs and Thomas*, 1977; *Prosser*, 1996; *Prosser and Soufi*, 1998]. In many mountainous regions, landslide hazard is directly proportional to the magnitude of vegetation loss [e.g., *Sidle et al.*, 1985]. Relative rates of root decay and regeneration appear to control the timing of the landsliding activity. For example, in the Idaho batholith, landslide activity increases significantly ~4 years after vegetation loss and continues to be high for ~6 more years [*Gray and Megahan*, 1981]. In the areas where summer months are hot and dry, as in the Idaho batholith, effects of wildfires on fluvial erosion are further elevated due to the formation of a water repellent layer in the topsoil that enhances runoff rates. Field observations documented the development of large rills and gullies shortly after wildfires triggered by high-intensity, short-duration summer thunderstorms due to both lowered erosion thresholds and increased runoff rates [e.g., *Megahan and Molitor*, 1975; *Meyer and Wells*, 1997; *Meyer et al.*, 2001; *Istanbulluoglu et al.*, 2003].

[5] Geomorphic processes supply large amounts of sediment and woody debris to streams. Although the short-term effects of forest disturbances are well documented in many locations, there is still a lack of information on their longer-term consequences [*Sidle et al.*, 1985]. *Kirchner et al.* [2001] suggested that human influence on erosion should be considered from two different perspectives. First, if human influences increase chronic erosion rates, they may result in significant harm to aquatic ecosystems that are naturally adjusted to episodic disruptions, and second, human activities may alter the size of the catastrophic events that deliver sediment to streams.

[6] Various internal (e.g., weathering rates, soil cohesion) and external (climate forcing, fires, etc.) factors influence the occurrence of episodic erosion events. Their significance and the risks associated with them can be recognized and managed when their frequency and magnitude and the physical factors contributing to their episodic behavior are known [*Selby*, 1993]. *Benda and Dunne* [1997a, 1997b] modeled the interactions between the stochastic sediment supply due to mass wasting driven by random rainstorms and fires and the topology of the channel network to generate spatial and temporal sediment fluxes and storages over large areas (~200 km^2) in the Oregon Coast Range. In a recent paper, *Lancaster et al.* [2003] developed a numerical model similar to *Benda and Dunne*'s [1997a, 1997b] to explore the influence of wood supply and transport on erosion, deposition, and sediment transport.

[7] In this paper, our specific emphasis is to explore the influence of forest vegetation and natural and anthropogenic vegetation disturbances on the frequency and magnitude of erosion events over thousands of years in a typical steep-forested headwater basin in the Idaho batholith under the current climate regime. We developed a physically based numerical model to explore the following questions: (1) How do forest stand density and productivity conditions, both manifested by different root cohesion values [*Sidle*, 1991], influence the magnitude and frequency of sediment yields? (2) How does disturbance, both natural (e.g., wildfires) and anthropogenic (e.g., forest management) alter the frequency and magnitude of sediment yields? (3) What is the influence of vegetation growth rates on erosion and recovery from disturbance? Disturbance impacts vegetation density and root cohesion and fires induce water repellence, all of which affect erosion and landslide initiation. The regrowth of vegetation following disturbance ameliorates these effects. The model was developed to explore and compare the frequency and magnitude of sediment production under undisturbed and disturbed conditions.

[8] The model characterizes the dominant erosion processes of the granitic mountains of central Idaho. In the area, diffusive processes such as soil creep, rain splash, and tree throw erode hillslopes and transport sediment to steep V-shaped headwater valleys, where sediment is temporarily stored and episodically evacuated by shallow landsliding, debris flows, and fluvial erosion [*Megahan et al.*, 1978; *Gray and Megahan*, 1981; *Kirchner et al.*, 2001]. Figure 1 shows a flow diagram of the processes represented in the model and the variables used to convey information between the various submodels. Model components are described in detail in section 3. The model uses digital elevation model (DEM) grid cells as model elements and operates on yearly time steps. Except for the geomorphic processes of soil evolution, gully erosion, and landsliding, all other modeled processes (i.e., fires, vegetation growth) are assumed spatially uniform. Soil depths are evolved in time due to the mass balance between soil production from underlying bedrock and the divergence of the sediment transport flux. Soil removal is modeled by fluvial erosion, landsliding, and debris flow scour. In the model, vegetation is grouped into overstory (e.g., trees) and understory (e.g., grass) vegetation cover types. Overstory vegetation is assumed to provide deep root cohesion, while the understory vegetation provides surface resistance to erosion. Timber harvest and wildfires are the types of disturbances modeled. In the model, both disturbances are assumed to completely remove the vegetation. In addition to this, wildfires are assumed to induce water repellence. Following vegetation disturbance, vegetation properties first decay and then recover in time to their predisturbed levels. The vegetation module simulates a yearly time series of the assumed spatially uniform response of vegetation-related variables (e.g., root cohesion, spatial average of overland flow vegetation roughness) to temporal occurrences of forest fires and forest harvests. The hydrology module characterizes
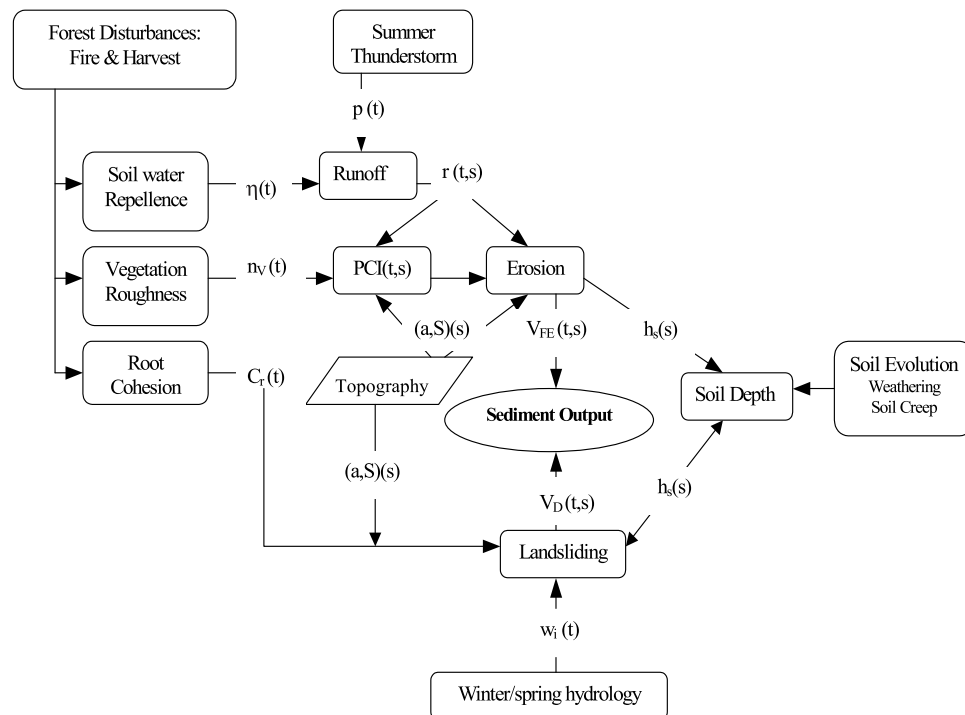
Figure 1. Model flow diagram. t and s represent variation in time and space, respectively, and PCI is the probability of channel initiation.

the driving factor for erosion and landslides using probability distributions of the largest summer thunderstorms and winter-spring water input events (that include snowmelt) and calculates assumed spatially uniform runoff rates and the wetness of the soil profile based on topography.

[9] The paper is divided into four additional sections. In section 2 we describe the geomorphology, hydrology, and different erosion patterns observed in our field area in the Idaho batholith. Section 3 first gives a brief overview of the physical processes that are considered in the model then describes the hydrologic response, hillslope mass transport and soil evolution, gully erosion, landslide and debris flow generation, and vegetation components of the model in greater detail. Initial conditions for model runs and the selection of parameter values are also reported in the end of section 3. Section 4 reports results from the model runs with varying root cohesion, with and without wildfires. Section 4 also compares simulated long-term average sediment yields and sediment yields from episodic erosion events in the study basin with reported long-term average and episodic sediment yields in the literature. Section 4 continues with a numerical paired watershed experiment, designed to compare the effects of fires versus harvest on sediment yields over management timescales. Section 5 is the conclusions section, where we briefly summarize the major findings in the paper.

2. Study Site

[10] The study area is a 3.9 km^2 watershed in the headwater drainages of Trapper Creek, within the north fork of the Boise River (NFBR) in the southwestern Idaho batholith (see Figure 2). This site was selected because

significant catastrophic erosion activity was observed and documented in the area following widespread stand-replacing wildfires in the last decade [*Meyer et al.*, 2001; *Istanbulluoglu et al.*, 2002, 2003]. Long-term sediment yields over 10,000 year timescales were also measured and reported by *Kirchner et al.* [2001] using cosmogenic ^{10}Be. Second, because of the distinct differences in the summer and winter-spring climate regimes (high-intensity, short-duration summer thunderstorms versus long-duration spring snowmelt events), both runoff erosion following wildfires during summer months and saturated colluvial failures triggered by spring snowmelt are historically observed in the area [*Megahan and Molitor*, 1975]. This allows exploration of the implications of both fluvial processes and mass movements on the frequency and magnitude of erosive response within the same model. We focused on the headwaters of Trapper Creek because it was an area that we could manageably survey and because it is small enough to assume a spatially uniform climate and soil and vegetation characteristics.

[11] The Idaho batholith consists of an extensive mass of granitic rock that covers a large portion of Idaho and some parts of Montana. In the study watershed, valleys are typically narrow and V shaped, with an average valley floor width of ~50 m. The elevation of the study watershed ranges from 1637 to 2231 m above sea level. The average slope is 47%, with a maximum of 98% in the study area. The colluvium is clay-poor and was produced due to the disintegration of Idaho batholith rocks [*Clayton et al.*, 1979; *Meyer et al.*, 2001]. It shows little or no cohesion and is subject to runoff erosion and mass wasting, especially following vegetation disturbances [*Gray and Megahan*, 1981].
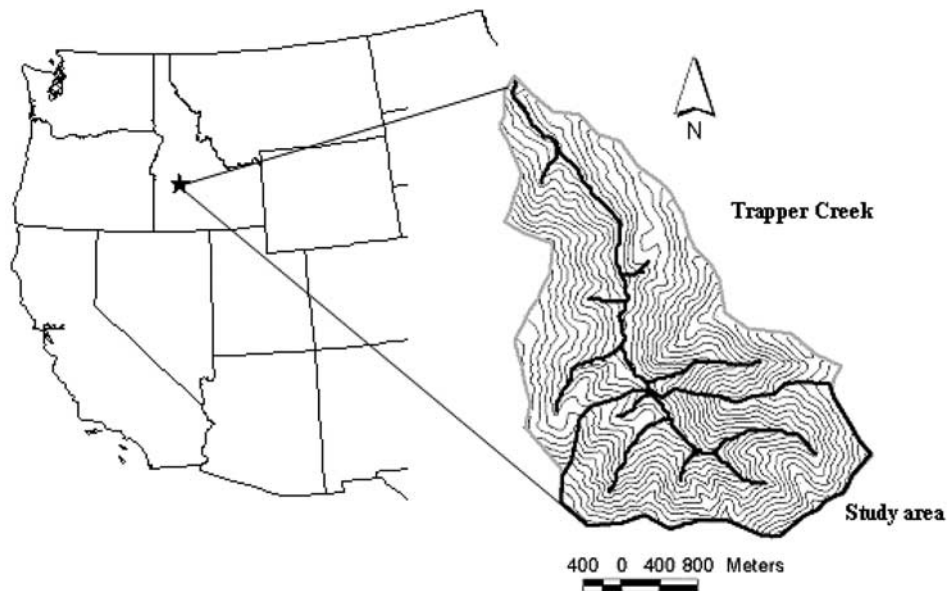
Figure 2. Location map of the Trapper Creek watershed and the study basin (outlined with the black solid line) in Trapper Creek. The contour interval is 30 m. Elevation ranges from 1637 to 2231 m.

[12] Stand-replacing wildfires are often considered to be one of the major causes of the episodic erosion in Idaho [*Clayton and Megahan*, 1997]. They are mostly weather related and are often ignited by lightning during summer drought conditions [*Barret et al.*, 1997]. The dominant overstory vegetation in the area is douglas fir and ponderosa pine, with an understory vegetation cover of mostly sage brush and grass. *Karsian* [1995] reports that in the current fire regime, spanning roughly the last 2000 years, natural stand-replacing fires have a probability of $P_F = 0.005$ in a given summer in this region.

[13] In the Idaho batholith, ~60–70% of the precipitation falls as snow during the winter. Snow accumulation usually starts in the second half of October and continues until March, when snowmelt starts. Snowmelt usually ends in April. Most of the remainder of the precipitation occurs as widespread, low-intensity, long-duration cyclonic storms in conjunction with snowmelt from March to May [*Megahan*, 1978; *Megahan et al.*, 1983; *Meyer et al.*, 2001]. In the summer-fall period, similar cyclonic storms may occur; however, high-intensity, short-duration convective storms are more common in this period. This type of storm usually produces localized heavy rainfalls in less than half an hour [*Meyer et al.*, 2001]. A storm intensity of 76 mm h^{-1} has a return period of 4 years in the central Idaho batholith [*Kidd*, 1964; *Clayton et al.*, 1979].

[14] The Idaho batholith summer and winter climate regimes cause two distinct erosion patterns. Erosive overland flow is uncommon in undisturbed forested basins [*Megahan*, 1983; *Clayton and Megahan*, 1997]. Water repellent soil formation following wildfires [*DeBano*, 1981; *Shakesby et al.*, 2000; *Benavides-Solorio and MacDonald*, 2001] significantly reduces the infiltration rates and promotes infiltration excess runoff generation, especially in dry summer months. Extreme gully erosion initiated by high-intensity thunderstorms is often observed during dry summer periods following forest fires [*Megahan*,

1992; *Meyer et al.*, 2001; *Istanbulluoglu et al.*, 2002]. Soil water repellence decreases or completely vanishes following prolonged rainy periods and spring snowmelts. During these wet periods, saturation overland flow may develop and initiate slope failures [*Clayton and Megahan*, 1997].

3. Model Formulation and Initial Conditions

3.1. Model Overview

[15] A diagram showing the model operation is given in Figure 1. In the model, forest disturbances alter three spatially constant, temporally variable parameters: (1) the impervious fraction of the basin due to fire-related soil water repellency (only for the case of fires); (2) overland flow vegetation roughness; and (3) root cohesion. The model starts with simulating the timing of fires (years with fire) stochastically, assuming a Poisson process for a specified duration of simulation. For the case of forest management, clear-cutting disturbances are modeled based on a fixed or variable rotation length. All disturbances are assumed to occur in the middle of summer. Vegetation growth starts from summer, and seasonal averages of vegetation-related parameters are calculated. Summer thunderstorms and winter-spring surface water input events are modeled independently using different probability distributions for the largest annual climate events observed in the respective seasons. The event sediment yield driven by these large climate events is interpreted as the total yearly sediment yield. Because episodic geomorphic events often scour the sediment stored in hollows, the probability of catastrophic erosion being triggered at the same site during the same year is very small and is neglected in the model. In the model, summer thunderstorms trigger gully erosion. Winter-spring water input increases pore pressures and triggers shallow landsliding and debris flows. Both fluvial erosion and mass wasting modify soil thickness along channels downslope. Spatially distributed soil evolution

due to soil production by bedrock weathering and erosion/deposition by soil creep occur continuously between erosion events.

3.2. Hydrology

3.2.1. Water Input

[16] In order to estimate the winter-spring water input rates, we analyzed 20 years of available daily meteorological data for winter-spring months from three sites at elevations 1688, 1703, and 1830 m ∼20 miles southeast of Trapper Creek (Atlanta stations). Daily water input rate, wi (mm d^{-1}), is calculated according to the difference between the snow depths, SD, in subsequent days multiplied by the ratio of snow density to the density of water, RSW, and adding the amount of precipitation, P, observed in the same day:

$$\text{wi} = (\text{SD}_{i-1} - \text{SD}_i)\text{RSW} + P_i \qquad \text{SD}_i < \text{SD}_{i-1} \quad (1)$$

$$\text{wi} = 0 \qquad \text{SD}_i \geq \text{SD}_{i-1}, \quad (2)$$

where i is the day for which water input is calculated. When there is an increase in the snow depth between two daily observations, the water input rate is taken to be 0, assuming that all the precipitation is in the form of snow. Equations (1) and (2) assume that snowmelt and precipitation rates are steady throughout the day and are constant over the watershed. The largest water input rate of each year is selected. The cumulative distribution of these largest events corresponded well with the extreme value type–I (Gumbel) distribution. In each yearly iteration of the model a random water input rate is generated from the Gumbel distribution and is used to calculate the maximum possible wetness parameter of the soil profile across the watershed. Because we are using yearly time steps in the model, all the pore pressure-induced landsliding and debris flow activities in a year are associated with the annual maximum water input event. A similar assumption was also made by *Benda and Dunne* [1997a].

[17] We selected the annual maximum of daily summer precipitation events from 50 years of observations available in the Idaho City climate station (elevation of 1208 m ∼15 km east of Trapper Creek) to characterize the extreme summer thunderstorms. These annual maximum daily values are used to obtain the parameters of the Gumbel distribution for summer thunderstorms. The analysis of daily water input alone does not provide information on storm duration. In order to approximate the durations associated with the thunderstorms, we used the nearest rain gauge that records 15 min precipitation (Lucky Peak Dam). This is further away, ∼64 km east of Trapper Creek, and is at a lower elevation (862 m). An exponential probability density function with a mean of 26 min fits the durations of all storms recorded at this location that occurred in the summer months (June–August) for the years 1972–2001.

[18] Similar to the winter-spring water input rates, one random thunderstorm each year is used to model gully incisions in the area. This neglects the contribution to erosion from thunderstorms smaller than the maximum event. The average event rainfall rate, $\bar{p}$, is calculated by dividing the total random precipitation depth, P, by storm duration, D:

$$\bar{p} = P/D. \quad (3)$$

In sampling from the exponential distribution for D, we censored the distribution to $D > 25$ min because an unreasonable $\bar{p}$ occurs if P is large and D is small.

[19] The climate forcing (annual maximum winter and summer water inputs and durations) is assumed to be a stationary random process. This assumption neglects any changes in the climate regime. It has been reported that in the western United States, mountain erosion rates are not sensitive to moderate climate changes [*Riebe et al.*, 2001].

3.2.2. Runoff Generation

[20] Considering the effects of soil disturbances on runoff generation, erosive runoff events are modeled by the infiltration excess runoff generation mechanism. Field observations of fire-related water repellency on small field plots show that water repellency may significantly increase runoff rates [*Walsh et al.*, 1998; *Shakesby et al.*, 2000]. However, there is not yet much field information available on the spatial contiguity of water repellency and its influence on watershed runoff generation [*Shakesby et al.*, 2000]. In the absence of detailed observations we assume that water repellent soils result in a fraction η of the watershed being impervious, with the remainder having an infiltration rate capacity I_c. The average instantaneous runoff rate over the area is the sum of runoff generated on both pervious and impervious watershed fractions according to

$$r = \begin{cases} (p - I_c)(1 - \eta) + p\eta & p > I_c \\ p\eta & p \leq I_c \end{cases}, \quad (4)$$

where p is the instantaneous precipitation rate.

[21] Rainfall rate is highly variable in time (e.g., in monthly and daily time periods, in individual storms, and during storms) and space [*Hutchinson*, 1995; *Schaake et al.*, 1996]. In a model of landscape evolution, *Tucker and Bras* [2000] showed that variability in the average storm rates results in higher erosion rates because of the nonlinearity of sediment transport to discharge. This led to higher drainage density and reduced relief in transport-limited catchments over geomorphic timescales. Similar to the variability in the average storm rates over the long term, temporal rainfall variability during storms which may trigger rapid fluctuations on the watershed hydrograph, especially in small basins, seems to be important for erosion modeling [*Smith et al.*, 1995]. Here we represented temporal rainfall variability during storms probabilistically. Gamma, exponential, Weibull, lognormal, and skewed normal distributions are among the probability distributions used to characterize rainfall variability at different timescales [*Eagleson*, 1978; *Yu*, 1998]. We used the exponential distribution to characterize rainfall rate variability during storms using the average rainfall rate given in equation (3):

$$F_P(p) = 1 - \exp\left(-\frac{p}{\bar{p}}\right). \quad (5)$$

$F_P(p)$ is the cumulative distribution function for rainfall rate p and gives the fraction of the storm duration when the

rainfall rate is $\leq p$ [*Yu*, 1998]. The probability density function of runoff rate r is derived from the probability distribution for p by solving equation (4) for p, $p = r + I_c$ $(1 - \eta)$ for $p > I_c$ and $p = r/\eta$ for $p \leq I_c$, and substituting p into equation (5), differentiating with respect to r:

$$f_R(r) = \begin{cases} f_{R1}(r) = (1/\eta\bar{p}) \exp\left(-\frac{r}{\eta\bar{p}}\right) & r \leq I_c\eta \\ f_{R2}(r) = (1/\bar{p}) \exp\left(-\frac{r+I_c(1-\eta)}{\bar{p}}\right) & r > I_c\eta \end{cases}. \quad (6)$$

The expected value of the distribution in equation (6) is the mean runoff rate:

$$\bar{r} = \int_0^{I_c\eta} r f_{R1}(r) dr + \int_{I_c\eta}^{\infty} r f_{R2}(r) = \bar{p}\left[\eta + e^{-I_c/\bar{p}}(1-\eta)\right]. \quad (7)$$

3.3. Hillslope Mass Transport

[22] Modeling the temporal and spatial variability of soil depths is crucial for long-term predictions of the frequency and magnitude of hillslope erosion, especially in mountainous settings [*Iida*, 1999]. In this model, soil development by bedrock weathering and soil gain or loss at a point due to continuous hillslope processes (i.e., soil creep, rain splash) are modeled based on the production rate of soil from the underlying bedrock and the downslope change in the rate of slope-dependent sediment transport, $q_s = -K\nabla z$, respectively. The conservation of mass equation for soil thickness is written as [*Tucker and Slingerland*, 1997; *Heimsath et al.*, 2001]

$$\left.\frac{\partial h_s}{\partial t}\right|_{chp} = -\frac{\rho_r}{\rho_s}\frac{\partial z_{b-s}}{\partial t} + \nabla(K\nabla z), \quad (8)$$

where h_s is the soil thickness, ρ_r and ρ_s are rock and soil bulk densities, respectively, z is the elevation of the soil surface, z_{b-s} is the elevation of the bedrock-soil interface, and $\partial_{zb-s}/\partial t$ is the lowering rate of the weathering front.

[23] In theory, the regolith production rate due to bedrock weathering is often assumed to be a function of soil depth [*Cox*, 1980; *Dietrich et al.*, 1995; *Heimsath et al.*, 1997]. In various empirical relationships the mechanical weathering rate usually decreases exponentially with soil thickness, while chemical weathering first increases with thickening soil, then attains a maximum value at some finite soil depth, and then decreases with further soil thickening. In seven different environments, *Heimsath et al.* [1997, 2001] used cosmogenic radionuclide measurements and topographic controls on soil depth to quantify the form of soil production function and consistently found that the soil production rate declines exponentially with increasing soil depth. In Heimsath's model, soil production is maximum on bare bedrock surfaces. On the basis of field evidence, largely in areas where the degradation of bedrock occurs through frost cracking, *Anderson* [2002] proposed a regolith production rule in which the bedrock weathering rate is set for a bare bedrock surface, then increases linearly with soil thickness up to a given depth, and then decreases exponentially beyond this finite depth. *Anderson* [2002] reproduced the formation of tors in high alpine surfaces in the Wind River Range, Wyoming, using this regolith production function.

[24] The distinctions between mechanical and chemical weathering in the Idaho batholith are obscure, and they complement each other synergistically [*Clayton et al.*, 1979]. We do not have sufficient field observations in the Idaho batholith area to test and calibrate different models for bedrock weathering. The exponential decline model [*Heimsath et al.*, 1997, 2001] has two empirical parameters, while the alternative model of *Anderson* [2002] has four empirical parameters. Rather than attempting to overcomplicate the model with difficult-to-estimate parameters, in this paper we assume that over the long term, bedrock weathering and sediment yield are in balance and thus use soil production equal to a constant rate of bedrock weathering obtained from denudation rates reported by *Kirchner et al.* [2001] for different catchments in the Idaho batholith. One consequence of this limitation is that at locations not subject to fluvial erosion and mass wasting processes, soil depth will progressively thicken indefinitely. In reality, steady state soil depths will be expected to develop on these planar and divergent slopes due to decreases in the bedrock weathering rate with increasing soil thickness. This indefinite thickening does not impact the results because in both our model and in the field episodic mass, movements are triggered on converging V-shaped hollows, where sediment input and soil thickening is dominated by slope-dependent transport (soil creep) entering the hollow from its sides. *Dietrich et al.* [1986], *Benda and Dunne* [1997a], and *Benda et al.* [1998] modeled slope-dependent sediment transport as the only source of sediment accumulation in the V-shaped hollows in the Oregon Coast Range. In the standard form of the slope-dependent transport function (equation (8)) that we use, sediment transport is not impacted by soil thickness. Section 3.7 gives details of our estimation of the slope-dependent transport (diffusion) coefficient and bedrock weathering rate.

3.4. Gully Erosion

[25] Field observations in the headwater basins in Idaho and in other mountainous parts of the western United States show that episodic erosion is associated with events that incise gullies upslope of existing perennial streams due to either overland flow erosion or to the initiation of landslides and debris flows. Sediment-water mixtures bulked in the upslope areas then enter the existing channels in the lower portions of the headwater basins and often scour them to bedrock as debris flows [e.g., *Benda and Dunne*, 1997a, 1997b; *Stock and Dietrich*, 2003] or hyperconcentrated flows [*Meyer et al.*, 2001; *Istanbulluoglu et al.*, 2003]. With this in mind, our objective is to model gully initiation in ungullied hillslopes and erosion in both incising gullies on hillslopes and in low-order streams. We used a probabilistic model to predict overland flow channel initiation on hillslopes driven by the largest annual thunderstorm of each year. The probability of channel initiation (PCI) at a point on the landscape is modeled as [*Istanbulluoglu et al.*, 2002]

$$\text{PCI} = \text{probability}(C \leq aS^\alpha) = \int_0^{a\alpha^a} f_C(C)dC, \quad (9)$$

where C is a threshold for channel initiation, f_C (C) is a probability density function describing random spatial

variability in C, α is a theoretical exponent for channel initiation due to overland flow, a is specific catchment area, and S is the topographic slope (sine of the slope angle) obtained from the DEM [e.g., *Tarboton*, 1997]. The same theory can be adapted for channel initiation due to different mechanisms, such as seepage erosion with relevant values for α and C [*Willgoose et al.*, 1991]. In this paper, C is derived theoretically for overland flow channel initiation. Derivation is based on the following assumptions: (1) channels are formed where effective shear stress of overland flow, τ_{fo} (shear stress acting solely on soil grains), exceeds a critical shear stress threshold for incipient motion, τ_c, ($\tau_{fo} > \tau_c$) [e.g., *Dietrich et al.*, 1993]; (2) overland flow is hydraulically rough, with the roughness independent of Reynolds number; and (3) overland flow velocity can be represented by Manning's equation. Effective shear stress for overland flow, τ_{fo}, is

$$\tau_{fo} = \rho_w g n_t^m q^m S^n f_s, \qquad (10)$$

where ρ_w is water density, g is gravity of acceleration, n_t is total Manning's roughness, and f_s is the shear stress partitioning ratio, which gives the fraction of shear stress acting on soil particles [*Foster*, 1982]. For overland flow, m and n are 0.6 and 0.7, respectively. It can be shown that when Manning's equation is used for overland flow velocity, the shear stress partitioning ratio is $f_s = (n_s/n_t)^{1.5}$, where n_s is Manning's roughness for bare soil [*Istanbulluoglu et al.*, 2003]. In this paper we assume that total roughness has two components: soil roughness, n_s, and vegetation roughness, n_V. We assume steady state hydrology, where discharge is proportional to runoff and specific catchment area, $q = ra$, and we use Shield's equation to characterize the critical shear stress for entrainment, $\tau_c = \tau_*(\rho_s - \rho_w)d_{50}$, where τ_* is dimensionless critical shear stress, ρ_s is sediment density, and d_{50} is the median grain size for the hillslope materials. Now, inserting the steady state hydrology assumption into shear stress in equation (10), equating equation (10) to the Shield's equation, and solving for area and slope, we get C as

$$C = \left(\frac{\tau_{*c}(\rho_s - \rho_w)d_{50}}{\rho_w g n_t^m \left(\frac{n_s}{n_t}\right)^{15}} \right)^{\frac{1}{m}} (1/r). \qquad (11)$$

In equation (11), $n_t = n_s + n_V$; here n_s is calculated as a function of median sediment size d_{50} from Strickler's equation [*Julien and Simons*, 1985] (for n_V, see section 3.6). In a deterministic model for channel initiation, channels incise when $\tau_{fo} > \tau_c$ or, as a topography-based threshold, when $aS^\alpha > C$, where $\alpha = n/m$. In the PCI theory, d_{50}, n_V, $n_s = f(d_{50})$, and r are random variables [*Istanbulluoglu et al.*, 2002].

[26] Here we employed a Monte Carlo simulation approach to calculate the mean and variance of the C thresholds, equation (11), to characterize the probability distribution of the spatial variability of C thresholds for each annual extreme storm event, using 1500 random numbers for d_{50} and n_V. The mean and variance of C are then used to parameterize a gamma distribution, used to represent PCI at each grid cell. The gamma distribution was shown to provide a reasonable match to the distributions of area-slope thresholds measured and modeled at channel heads in the field [*Istanbulluoglu et al.*, 2002]. Although *Istanbulluoglu et al.* [2002] modeled the spatial variability in r using a uniform distribution for a thunderstorm event in Trapper Creek, here we ignored the spatial variability in r and took the mean runoff rate, equation (7), as a constant input in the Monte Carlo procedure for each annual storm event. Uncertainty in n_s is characterized using field observations of median sediment sizes that showed a lognormal distribution [*Istanbulluoglu et al.*, 2002] in Trapper Creek. Vegetation is subject to wildfire and harvest disturbances; therefore n_V exhibits temporal variations due to the interaction between the rate and magnitude of disturbances and the vegetation regrowth rate. We model the temporal variability in the spatial average $\overline{n_V}$ for each time step (year). Spatial variability in vegetation roughness is characterized using a uniform distribution between upper and lower bounds that average to the $\overline{n_V}$ modeled for each summer. *Istanbulluoglu et al.* [2002] used uniformly distributed vegetation roughness values between 0.015 and 0.1, which describe a $\pm73.4\%$ deviation from the mean value of 0.0575. Assuming that the $\pm73.4\%$ deviation is constant for every summer, the maximum value for vegetation roughness is calculated by $\overline{n_V} + 0.734\,\overline{n_V}$ and the minimum value by $\overline{n_V} - 0.734\,\overline{n_V}$. These bounds are used in the uniform distribution to generate vegetation roughness.

[27] The channel initiation theory is applicable in unchanneled upland areas above perennial stream heads. Perennial drainages exist in the field even during times when runoff is insufficient to cause any erosion. To distinguish gullies from the perennial streams in the study watershed, we defined an upper boundary for the C threshold, C_F, that captures the existing streams. Thus when $C \geq C_F$, threshold theory would predict the existing network. An existing network is defined by referring to Robert E. Lee Creek, a neighboring drainage to Trapper Creek that was not significantly influenced by recent wildfires [*Istanbulluoglu et al.*, 2002]. On the basis of field observations of seepage and saturation excess overland flow, we found that a channel initiation threshold, $C_F = 500$ m, used with $aS^\alpha > C_F$ mapped the channels in Robert E. Lee Creek from the DEM. Episodic erosion is assumed to only occur in years when the average of the 1500 simulated C values, which depend on the runoff rate r (equation (11)), is $< C_F$. In these years a PCI grid is defined for each simulated thunderstorm, and erosion is calculated using the method given below in both uplands and existing channels. This links erosion in the existing drainages to episodic gully erosion events in the uplands and ignores erosion in the channel network between episodic events. We assume that erosion, if observed between episodic incision, contributes to the day-to-day sediment yields.

[28] For channels where easily detachable noncohesive material is available, flow is assumed to be at its sediment transport capacity, and the erosion amount from a location would be equal to the excess (downstream change) of sediment transport capacity [*Willgoose et al.*, 1991; *Tucker and Bras*, 1998]:

$$-\left.\frac{\partial h_s}{\partial t}\right|_{fluvial} = \frac{\rho_s}{\rho_b} \nabla q_s, \qquad (12)$$

where q_s is unit sediment discharge ($L^2 T^{-1}$) and ρ_b is soil bulk density. Erosion calculated using equation (12) multiplied by the storm duration gives a potential depth of erosion at a point. In the model, this potential is compared with soil depth, and actual erosion is calculated as the minimum of either potential erosion or the soil depth.

[29] The instantaneous sediment discharge capacity in a channel can be modeled as a nonlinear function of shear stress in excess of a threshold

$$Q_s = \gamma W_f (\tau_f - \tau_c)^{p_f}, \qquad (13a)$$

where

$$\gamma = \frac{\kappa \sqrt{g(s-1)d_{50}^3}}{(\rho_w g(s-1)d_{50})^{p_f}}, \qquad (13b)$$

Q_s is the volumetric sediment discharge ($L^3 T^{-1}$), τ_f is effective shear stress of concentrated flow in channels, τ_c is critical shear stress, γ is a transport coefficient, κ is a calibration constant, W_f is flow width, d is sediment size, and p_f is an exponent that is typically 1.5 for bed load and higher for total load equations [*Garde and Raju*, 1985]. Assuming steady, uniform flow and using Manning's equation for flow velocity, flow width, and effective shear stress, equation (13a) can be written as a power function of steady state discharge (excess rainfall times drainage area). For the case of $\tau_c = 0$, sediment transport capacity then becomes

$$Q_s = \langle \gamma \chi_w \chi_\tau^{p_f} \rangle (rA)^M S^N, \qquad (14)$$

where the parameters χ_w and χ_τ are constants that relate discharge and slope to flow width and shear stress and are related to channel cross section shape and the latter to both channel shape and roughness. A is drainage area, and M and N are exponents. *Istanbulluoglu et al.* [2003] reports derivations for the constants of this functional form and calibrates the empirical exponents of the model using field observations in Trapper Creek. Here we assume that when erosion starts, it scours the vegetation cover, and we thus set $\tau_c = 0$ for sediment transport in gullies. This is verifiable with our field observations in the Idaho batholith. First, episodic erosion is often linked to vegetation removal, which decreases the channel initiation threshold so that there is less concern of shear stress partitioning due to vegetation. Second, even in the presence of vegetation, once incisions start, concentrated flow in gullies produces shear stresses high enough to scour both soil and vegetation cover at the same time.

[30] For a given storm, the expected value of the sediment transport rate at each point is obtained by integrating the instantaneous sediment transport capacity function (equation (14)) over the probability distribution of runoff during the storm, equation (6), and multiplying with the PCI:

$$\bar{Q}_s = \text{PCI} \int_0^\infty Q_s f(r) dr = \left\langle \gamma \chi_W \chi_\tau^{p_f} \int_0^\infty r^M f_R(r) dr \right\rangle A^M S^N \text{PCI}. \qquad (15)$$

This integral is solved analytically. Here we report the equation as a function of a parameter that absorbs all the hydrologic and hydraulic variables, χ_{Q_s}, and topographic variables A, S, and PCI as

$$\bar{Q}_s = \chi_{Q_s} A^M S^N \text{PCI}, \qquad (16)$$

where

$$\chi_{Q_s} = \gamma \chi_W \chi_\tau^{p_f} \bar{p}^M \left[\eta^M \Gamma\left(M+1, \frac{I_c}{\bar{p}}\right) + e^{-I_c(1-\eta)/\bar{p}} \left(\Gamma(M+1) \right. \right.$$
$$\left. \left. - \Gamma\left(M+1, \frac{I_c \eta}{\bar{p}}\right) \right) \right], \qquad (17)$$

where $\Gamma()$ is the gamma function and $\Gamma(,)$ is the incomplete gamma function [*Benjamin and Cornell*, 1970]. In equations (9) and (15), PCI is a function of r. PCI calculates the probability of channel initiation assuming overland flow conditions for a given storm, considering spatial variability in its parameters. We assume that once a channel is incised, it will continue to exist during a storm event despite fluctuations in runoff rate. Therefore we used PCI as a function of $\bar{r}$ from equation (7) rather than including it in the integral in equation (15). A similar derivation for the long-term averages of sediment transport rates driven by stochastic storms was given by *Tucker and Bras* [2000]. Our derivation, although similar in spirit, includes aggregation of the effects of rainfall variation during storms, water repellent soil formation, and probability of channel initiation.

3.5. Landsliding and Debris Flows

[31] Recent technology for the mapping of landslide susceptibility uses the infinite slope stability equation to map the areas prone to shallow landsliding based on DEMs [*Montgomery and Dietrich*, 1994; *Wu and Sidle*, 1995; *Pack et al.*, 1998]. The infinite slope stability model we used is in the form given by [*Pack et al.*, 1998]:

$$\text{FS} = \frac{C_r + C_s}{h_s \rho_b g \sin\theta} + \frac{\cos\theta \tan\phi[1 - R_w \rho_w/\rho_b]}{\sin\theta}, \qquad (18)$$

where FS is factor of safety, i.e., the ratio of resisting to driving forces, C_r and C_s are root and soil cohesion, respectively, h_s is the soil thickness perpendicular to slope, θ and ϕ are ground slope angle and soil internal friction angle, respectively, and R_w is the relative wetness, which is defined as the ratio of subsurface flow depth flowing parallel to the soil surface to soil thickness. Assuming that lateral discharge at each point is in equilibrium with a steady state water input rate, wi ($L T^{-1}$), and that the capacity for lateral water flux at each point is $K_s h_s \sin\theta$, where K_s is the lateral saturated hydraulic conductivity ($L T^{-1}$) of the soil, R_w is written as the ratio of lateral discharge to the lateral flux capacity:

$$R_w = \min\left(\frac{wi a}{K_s h_s \sin\theta}, 1\right). \qquad (19)$$

The relative wetness has an upper bound of 1, with any excess assumed to be saturation excess overland flow.

[32] In the V-shaped hollows of the Idaho batholith, landslides are mostly triggered by spring snowmelt and

rain-on-snow events when the hollow axis is saturated. This saturated slide material often triggers a debris flow that erodes the hollow axis to bedrock or flows in preexisting gullies [*Megahan et al.*, 1978]. In the model we assumed that all the unstable elements where FS < 1 produce landslides that trigger debris flows and completely scour the colluvium to bedrock. This assumption is consistent with the field observations both in the Idaho batholith [*Megahan et al.*, 1978], in the western United States, and in Taiwan [*Benda and Cundy*, 1990; *Stock and Dietrich*, 2003]. Debris flows are routed downhill in the steepest direction toward one of the eight surrounding grid cells. No debris flow deposition is allowed in the model because of the steep topography that is well above threshold angles reported for debris flow deposition [*Benda and Cundy*, 1990; *Benda and Dunne*, 1997a]. Allowing deposition would further complicate the model as there is significant uncertainty associated with modeling debris flow deposition [*Lancaster et al.*, 2003]. This assumption is consistent with field observations in our study basin, where a brief high-intensity, short-duration thunderstorm event a year after a wildfire triggered extensive upland gullying that formed a hyperconcentrated flow downstream, scouring the part of the main channel of the study area used in the paper [*Istanbulluoglu et al.*, 2002, 2003].

3.6. Vegetation Component

[33] Vegetation roots tend to stabilize the slopes by providing root cohesion. In the infinite slope stability model, factor of safety, FS (equation (18)), is linearly proportional to root cohesion. Similarly, field observations show that the presence of surface vegetation cover protects the land from erosion by increasing the erosion thresholds [*Prosser and Dietrich*, 1995]. In the PCI theory the channel initiation threshold increases as a function of vegetation roughness (see equation (11)). Here we modeled the death and regrowth of tree roots that provide deep root cohesion and vegetation cover. We also modeled the temporal behavior of the water repellent impermeable watershed fraction, η, by relating the recovery of hydrophobicity to vegetation cover spread. We divided the vegetation into two groups, overstory and understory vegetation. Root cohesion provided by the understory vegetation is ignored due to its relatively lesser contribution, and the understory vegetation cover is assumed to provide additional roughness on the surface that enhances the surface resistance to erosion.

3.6.1. Root Cohesion

[34] The net root strength of a forested hillslope parcel subject to vegetation removal is the sum of decaying root cohesion due to the removed trees and regeneration of the root cohesion by new growing plants [*Sidle*, 1992]. The dimensionless root strength decay following vegetation disturbances can be estimated by a negative exponential function [*Burroughs and Thomas*, 1977; *Sidle*, 1992]:

$$D_r = \exp(-k_C t^{n_C}), \qquad (20)$$

where D_r is dimensionless root strength decay ($0 < D_r \leq 1$), t is time since the vegetation removal, and k_C and n_C are vegetation-dependent empirical constants. *Sidle* [1991,
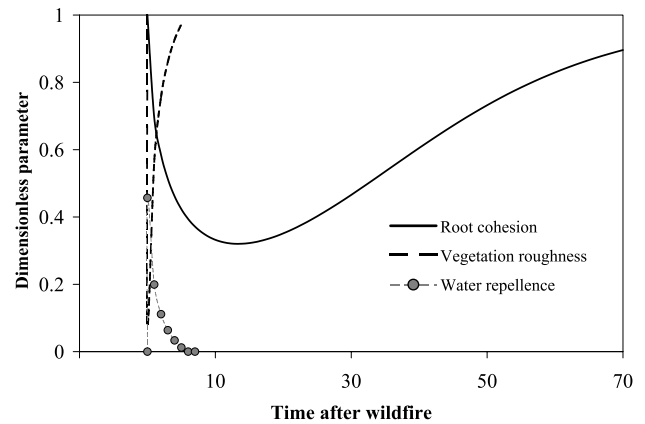
Figure 3. Vegetation response to wildfire disturbances based on the vegetation model parameters reported in Table 1 selected for Idaho batholith conditions. Time is in years.

1992] described the rate of root regrowth of planted or invading vegetation by a sigmoid curve:

$$R_r = c_C + 1/(a_C + b_C \exp(-\mathrm{x}_C t)), \qquad (21)$$

where R_r is the dimensionless root strength recovery ($0 < R_r \leq 1$) and a_C, b_C, c_C, and ξ_C are empirical constants. The total root cohesion following vegetation death is

$$C_r(t) = C_{\mathrm{pre}} D_r(t) + C_m R_r(t). \qquad (22)$$

In equations (21) and (22), t is the time after disturbance, C_{pre} is the root cohesion at the time of vegetation disturbance, and C_m is mature root cohesion. Equation (22) says that as the root cohesion of the disturbed trees decay from a predisturbed cohesion value, vegetation invading the site starts producing cohesion and can grow up to maturity (Figure 3).

3.6.2. Vegetation Roughness

[35] Vegetation increases the total flow roughness and reduces the fraction of shear stress acting solely on soil grains. A very simple approach to calculate vegetation roughness is used in this paper. For a more sophisticated physical approach the reader is directed to *Freeman et al.* [2000].

[36] In order to model the influences of the understory vegetation on erosion rates over time, we first related vegetation cover conditions to overland flow vegetation roughness, n_V; and, second, developed a theory to model the temporal variations in the understory vegetation cover to obtain temporal dynamics of vegetation roughness. The flow roughness coefficients for stream channels and water conveyance structures under different channel cover material, shape, irregularity, etc. have been documented [*Chow*, 1959; *Arcement and Schneider*, 1984]. However, very few data sets exist for shallow overland flow roughness on natural surfaces. Overland flow roughness values obtained from experimental studies are often classified for different surface cover and treatment conditions such as sparse, poor, good vegetation cover, etc. [*Ree et al.*, 1977; *Engman*, 1986]. These observations suggest a connection between

cover density and roughness. On the basis of this field evidence, we start with assuming that surface roughness provided by a certain type of vegetation can be considered proportional to its fractional ground cover, F_{gc}, $n_V \propto F_{gc}$, which could range from 0 to a maximum value under optimum growth conditions $F_{gc} \leq \max(F_{gc}) \leq 1$. We further assume that the proportionality of fractional ground cover of a vegetation type to the fractional ground cover of a reference vegetation, F_{gc}^R, that has a known roughness coefficient n_v^R is equal to the fraction of their roughness values:

$$\frac{F_{gc}}{F_{gc}^R} = \frac{n_v}{n_v^R}. \tag{23}$$

This assumption allows us to estimate the roughness of any type of vegetation from its ground cover by comparing it to the fractional cover of the reference vegetation:

$$n_v = n_v^R \frac{F_{gc}}{F_{gc}^R}. \tag{24}$$

Here dense forest cover is selected as the reference vegetation, and its fractional ground cover is assumed to be 1.

[37] After vegetation is disturbed, it will regrow in time, and the surface resistance to erosion will gradually recover to prefire levels. This regrowth time frame may range from several months to years, depending on the vegetation and site conditions [*Megahan and Molitor*, 1975; *Prosser and Soufi*, 1998; *Prosser and Williams*, 1998]. The rate of biomass regrowth is often related to soil productivity, seasonal and site-specific conditions such as temperature and soil moisture, solar radiation, available plant biomass, and ground cover density [*Alberts et al.*, 1989; *Arnold et al.*, 1995]. Here we took a very simple approach to modeling surface vegetation growth. We ignored the influences of seasonal and site conditions to the biomass growth rate and assumed that the rate of biomass growth, dB_m/dt, is proportional to a potential rate of biomass growth rate on a bare soil, k_B, and the existing vegetation ground cover fraction according to

$$\frac{dB_m}{dt} = k_B k_V \left(1 - F_{gc}\right), \tag{25}$$

where k_V is a parameter to relate the available bare soil surface to the growth rate (e.g., D. B. G. Collins et al., Modeling the effects of vegetation-erosion coupling on landscape evolution, submitted to *Journal of Geophysical Research*, 2003). Equation (25) says that the biomass growth rate will be relatively fast immediately after a vegetation disturbance (i.e., because of the availability of soil supplies necessary for plant growth) and that it will approach zero as the ground is fully covered with vegetation (i.e., owing to the competition for supplies).

[38] In the Water Erosion Prediction Project (WEPP) model [*Alberts et al.*, 1989; *Arnold et al.*, 1995] an exponential relationship is used to relate vegetation canopy cover, plant height, and plant ground cover to vegetation biomass. Fractional ground cover as a function of biomass is written as

$$F_{gc} = 1 - e^{-B_m B_c}, \tag{26}$$

where B_c is a plant-related constant. Substituting equation (26) into equation (25) gives the rate of biomass growth as a function of available biomass. Assuming that disturbance completely removes the understory vegetation ($B_m = 0$ at $t = 0$), the initial value problem can be solved by separating variables and integrating to give

$$B_m = \frac{1}{B_c} Ln(k_B k_V B_c t + 1). \tag{27}$$

Now, substituting equation (27) into equation (26) gives the fractional ground cover as a function of time following vegetation death:

$$F_{gc}(t) = 1 - 1/(k_B k_V B_c t + 1), \tag{28}$$

and substituting equation (28) into equation (24) and limiting the fractional ground cover to a maximum value that the plants can cover, Manning's roughness of understory vegetation as a function of time can be written as

$$n_v(t) = n_v^R \frac{\min\left[1 - 1/(k_B k_V B_c t + 1), F_{gc}^{max}\right]}{F_{gc}^R}. \tag{29}$$

3.6.3. Fire Occurrence and Water Repellent Soil Formation and Recovery

[39] Here a very simple approach is used to describe the occurrence of spatially uniform fires and to model water repellency and its effects on runoff generation and soil erosion that are also assumed spatially uniform in a basin. The occurrence of fires is modeled using a Poisson process, with equal probability of wildfires, P_F, in each year. We assume that water repellence due to wildfires is only experienced by some fraction of a devegetated surface, R_f, drawn from a uniform probability distribution. We write the postfire pervious fraction, P_f^{post}, of a burnt area as a reduced fraction of its prefire pervious fraction, P_f^{pre}, as

$$P_f^{post} = P_f^{pre}\left(1 - R_f\right). \tag{30}$$

We assume that as vegetation grows on a devegetated impervious surface, vegetation roots will break the water repellent layers, form preferential microchannels, and enhance the infiltration rates [*Shakesby et al.*, 2000]. Therefore the impervious fraction of an area after a wildfire, $(1 - P_f^{post})$, will gradually recover in time as the ground cover increases, and it is completely removed when the ground cover fraction attains its maximum possible value. Changes in the pervious fraction following wildfires is therefore modeled based upon the vegetation recovery equation (28) as

$$P_f(t) = P_f^{post} + \frac{\min\left[1 - 1/(k_B k_V B_c t + 1), F_{gc}^{max}\right]}{F_{gc}^{max}}\left(1 - P_f^{post}\right), \tag{31}$$

Table 1. Constant Model Parameter Values Used in Simulations

Parameter	Value
Mean summer precipitation depth, $\bar{P}$, mm, and duration, $\bar{D}$, h	21.6, 0.5
Mean winter water input rate, $\overline{wi}$, mm d^{-1}	42
Parameters of the Gumbel[a] distribution, u, α	
Winter-spring water input, mm d^{-1}	0.655, 3
Summer thunderstorms, mm d^{-1}	0.0508, 47.88
Dimensionless infiltration capacity, $I_c/(\bar{P}\bar{D}^{-1})$	10
Saturated lateral hydraulic conductivity, K_s, m d^{-1}	60
Weathering rate constant, $\partial z_{b-s}/\partial t$, m yr^{-1}	1.1×10^{-4}
Diffusion constant, K, m^2 yr^{-1}	4×10^{-4}
Rock, sediment and soil bulk density, ρ_r, ρ_s, kg m^{-3}	2650, 1500
Sediment transport rate constant and exponent, κ, p_f	20, 3
Transport coefficient, γ, m^5 s^5 kg^{-3}	1.15×10^{-7}
Shear stress constant, χ_c, kg m$^{-2.8}$ s$^{-1.4}$	303
Flow width constant, χ_w, m$^{0.1}$ s$^{0.3}$	0.9
Median size of sediment in transport, d, mm	3
Internal friction angle, ϕ, deg	38
Mature root cohesion, C_m, kPa	9
Root strength parameters for decay, k_C, n_C	0.376, 0.595
Root strength parameters for regrowth, a_C, b_C, c_C, ξ_C, yr^{-1}	0.85, 4.71, -0.18, 0.057
Overland flow roughness for mature forest, n_V^m	0.8
Maximum fractional ground cover, max(F_{gc})	0.8
Biomass growth rate on a bare surface, k_B, kg m^{-2} yr^{-1}	1.4
Plant related constant, B_c, kg^{-1}	1
Probability of wildfire, P_F	0.005

[a]Cumulative distribution function for Gumbel distribution is $F_x(x) = \exp[-e^{-\alpha(x-u)}]$.

and the impervious fraction of the watershed, η, is

$$\eta(t) = 1 - P_f(t). \qquad (32)$$

η is used in equations (6), (7), and (17) to relate fire-induced water repellency to runoff generation and erosion processes.

[40] The vegetation model is calibrated based on the field observations of vegetation response to disturbances in the Idaho batholith. Figure 3 shows an example of the vegetation response to wildfire disturbances by plotting the dimensionless root cohesion of equation (22), vegetation roughness (as the ratio of fractional ground cover recovery in time, equation (29), to the fractional ground cover prior to wildfires), and water repellency (as a water repellent fraction of watershed area, equation (32)) based on the model parameters given in Table 1, selected to be representative of the region (see section 3.6). In the example, fire consumes all the vegetation at $t = 0$. The destruction of the surface vegetation biomass abruptly brings down the vegetation roughness to a selected residual value and causes water repellency. Understory vegetation typically recovers within several years following wildfires and breaks the water repellent soil layers (Figure 3), as was suggested by field observations [*Benavides-Solorio and MacDonald*, 2001; *Megahan*, 1992]. During the understory vegetation recovery period, significant soil erosion may be observed due to low surface roughness values that increase the fraction of shear stress acting on soil grains and enhance runoff generation due to water repellency [*Wells*, 1987; *Cannon et al.*, 1998; *Benavides-Solorio and MacDonald*, 2001; *Moody and*

Martin, 2001]. Root cohesion produced by trees attains the lowest levels in 10 years following the wildfire and leaves the land susceptible to landsliding and debris flow generation [*Megahan et al.*, 1978; *Gray and Megahan*, 1981]. Finally, ~80% of the mature root cohesion recovers by the end of 60 years after tree death. Many field observations show that erosion is concentrated in the first 20–30 years following wildfires (Figure 3) during the vegetation recovery period. This period is often known as the accelerated erosion period (AEP), and its length depends on the rate of root cohesion decay and recovery and the arrival of high-magnitude climate events when the root cohesion value is relatively low [*Gray and Megahan*, 1981; *Megahan*, 1992].

3.7. Initial Conditions and Parameter Values

[41] We present the model parameter values that we think best represent the climate, erosion, and vegetation conditions in the Idaho batholith, in particular, our study watershed, based on the available data in the area (Table 1). In some of the following model runs, parameters that are related to vegetation have been altered to simulate the influence of vegetation on sediment yields. These parameters are described, when required, in the paper.

[42] Climate parameters are obtained from the climate data available in the area (described in section 3.1). The infiltration capacity is represented in a nondimensional form relative to the average storm rainfall rate as the ratio $Ic/\bar{p}$, where $\bar{p} = (\bar{P}\bar{D}^{-1})$. This ratio is taken to be 10. This gives $I_c \cong 400$ mm h^{-1}. This infiltration rate means that the average thunderstorm rainfall rate does not produce runoff when the impervious fraction of the watershed, η, is 0. This is consistent with the field observations in the area, where summer thunderstorms rarely generate direct runoff under forested conditions [*Megahan*, 1983].

[43] Lateral flow transport in the soil is controlled by the saturated lateral hydraulic conductivity, K_s. Saturated lateral hydraulic conductivity may vary by orders of magnitude in the field on the hillslope scale [*Nielsen et al.*, 1973; *Moore et al.*, 1986]. In our model the smaller (or higher) the K_s, the higher (or lower) the frequency of failures. Landslides and debris flows remove soil from hillslopes. Therefore an increase in K_s in the model allows thicker soil depths to develop or vice versa. Here we calibrated K_s by running simulations with different K_s values and selected $K_s = 60$ m d^{-1}. This is a hillslope-scale hydraulic conductivity and averages the effects of root channels and layers with different hydraulic conductivity values in the soil profile. For comparison, *Montgomery et al.* [2002] reported saturated lateral hydraulic conductivity values from 8 to up to 86.4 m d^{-1} in the Oregon Coast Range.

[44] No field observation exists for the long-term bedrock weathering rates in our field area. Long-term average weathering rates may be inferred from the sediment mass balance of watersheds, assuming that under dynamic equilibrium the sediment carried away from the basin is equal to the amount produced from bedrock [*Clayton and Megahan*, 1986; *Kirchner et al.*, 2001]. Here we used a constant denudation rate of 1.1×10^{-4} m yr^{-1} for bedrock weathering. This value is the average of the denudation rates reported for some watersheds in the Idaho batholith that are close to the size of our study area [*Kirchner et al.*, 2001].

[45] The diffusion constant was estimated from field observations by solving the slope-dependent linear sediment transport equation, $q_s = KS$, for the diffusion constant, K, using estimated sediment fluxes, q_s, from dated colluvium samples. When surveying the sample sites, slope gradients were measured over distances commensurable to those estimated from the DEMs with the intent that the numbers obtained could be used directly with a DEM to model soil flux volumes. Diffusion constants were found in the range of $1 \times 10^{-4} - 9 \times 10^{-4}$ m^2 yr^{-1}, with an average rate of 3×10^{-4} m^2 yr^{-1}. Experimenting with different diffusion constant estimates from field observations and bedrock weathering rates taken from reported denudation rates from *Kirchner et al.* [2001] in the model, we found that $K = 4 \times 10^{-4}$ m^2 yr^{-1} gives reasonable bedrock exposure patterns (on sharply curved ridge tops and topographic noses) over the study watershed, and therefore we used this value in all simulation runs. With this selected diffusion constant and bedrock weathering rate, soil flux into a typical V-shaped hollow in the field due to soil creep from its sides (total flux $= 2KS$, where $S = 0.3$ on the average) accounts for ~70% of soil thickening in the hollows.

[46] Parameters of the fluvial sediment transport model which relate shear stress and gully width to discharge and slope, χ_c and χ_W, respectively, are obtained from *Istanbulluoglu et al.* [2003], where greater detail can be found on the derivation of these parameters. A parabolic flow cross section with a constant width-to-depth ratio of 2 is used. The soil internal friction angle is taken as 38° based on *Hampton et al.* [1974].

[47] Manning's roughness value of 0.8 for timberland with deep forest litter and dense grass was reported by *Huggins and Burney* [1982]. *Engman* [1986] reported an overland flow Manning's roughness of up to 0.66 for grass. We took 0.8 for the reference Manning's roughness coefficient for overland flow (equations (23) and (29)). *Clayton and Megahan* [1997] reported ground cover fractions of an undisturbed forest floor in the south central Idaho batholith for a period of 4 years in the range of 0.2–1, with an average of 0.8. In the model we set the maximum fractional ground cover of the understory vegetation (equation (29)) to 0.8. This predicts that when the understory vegetation grows to maturity, it will provide a vegetation roughness of 0.64.

[48] Root strength parameters for decay ($k_C = 0.376$, $n_C = 0.595$), regrowth ($a_C = 0.85$, $b_C = 4.71$, $c_C = -0.18$, $\xi_C = 0.057$ yr^{-1}), and mature cohesion ($C_m = 9$ kPa) of the root cohesion model are selected for Rocky Mountain douglas fir [*Burroughs and Thomas*, 1977; *Sidle*, 1991]. We used the potential rate of understory vegetation biomass growth on a bare surface, $k_B = 1.4$ kg m^{-2} yr^{-1} in equation (25). This biomass growth rate, with $B_c = 1$ kg^{-1}, provides a postfire fractional ground cover recovery of 80% (equation (28)) in the third year following wildfires, as was suggested in field observations [*Meyer et al.*, 2001; *Benavides-Solorio and MacDonald*, 2001].

[49] The probability of the occurrence of stand-replacing wildfires in Trapper Creek in a given year is estimated as $P_F = 0.005$, based on observations [*Karsian*, 1995; K. Geier-Hayes, personal communication, 2001]. This corresponds to a 200 year average fire recurrence interval. It is important here to note that in this model we do not model ground fires. We do not have field observations to suggest

that ground fires cause significant geomorphic response. There is also a lack of field data that reports, for example, what fraction of the vegetation is burned during ground fires, how hot they can get to cause water repellence, and how vegetation recovers following small fires. With all these uncertainties we assume that only stand-replacing fires alter root cohesion and surface roughness and cause water repellence. In similar modeling studies, *Benda and Dunne* [1997a, 1997b] and *Lancaster et al.* [2003] also modeled only stand-replacing fires in the Oregon Coast Range.

[50] Some water drop tests conducted by the U.S. Department of Agriculture Forest Service Rocky Mountain Research Station in Boise, Idaho, on water repellent soils shortly after the Trail Creek fire in Atlanta (~20 miles southeast of Trapper Creek) in the summer of 2001 showed water repellency at up to 90% of the sample points. On the basis of this information, we set the upper bound of the uniform distribution for the water repellent fraction R_f to 0.9, and we used 0.4 for the lower bound.

[51] We obtained an initial condition for soil depths by allowing soil evolution by diffusion and bedrock weathering over 3000 years (as in, e.g., *Dietrich et al.* [1995]). This procedure fills the hollows with colluvium and develops thinner soils on the ridges. In each of the simulations described in section 4 the model is run for 10,000 years. The first 3000 years in each simulation is taken as a spin-up period to limit the sensitivity to the initial conditions.

[52] In what follows, we explore the sensitivity of sediment yield to forest vegetation. We first assume a constant root cohesion parameter (i.e., no root disturbance). Under this assumption the triggering mechanism for erosion and mass movements is the combination of climate forcing and the thickening of colluvium. Second, we model the effects of forest fires on sediment yields by simulating random wildfires that kill all the vegetation. The model is run for 7000 years for both cases using the same climate events. Following the sensitivity analysis, we compare the mean episodic event sediment yields (mean ESY) and the long-term annual averages (LASY) of the simulation results against field observations to assess the performance of our model. We then use our model to compare the effects of forest harvest and wildfires on basin sediment yields to gain more insights on vegetation-erosion interactions under different disturbance patterns.

4. Results and Discussions
4.1. Influence of Forest Vegetation and Wildfires on Sediment Yields

[53] We performed four simulations with progressively increasing root cohesion. We used a root cohesion of 1 kPa to characterize low forest density with poor forest growth conditions and then used minimum, average, and maximum mature root cohesion values 4, 9, and 14 kPa, respectively, to characterize progressively increasing site productivity conditions that develop a progressively higher forest stand density for Rocky Mountain douglas fir (dominant vegetation in the area) [*Burroughs and Thomas*, 1977]. Second, we considered the effects of forest fires on the episodic nature of sediment yields.

[54] A 10,000-year-long data set for climate events and years with wildfires was generated. All of the simulations
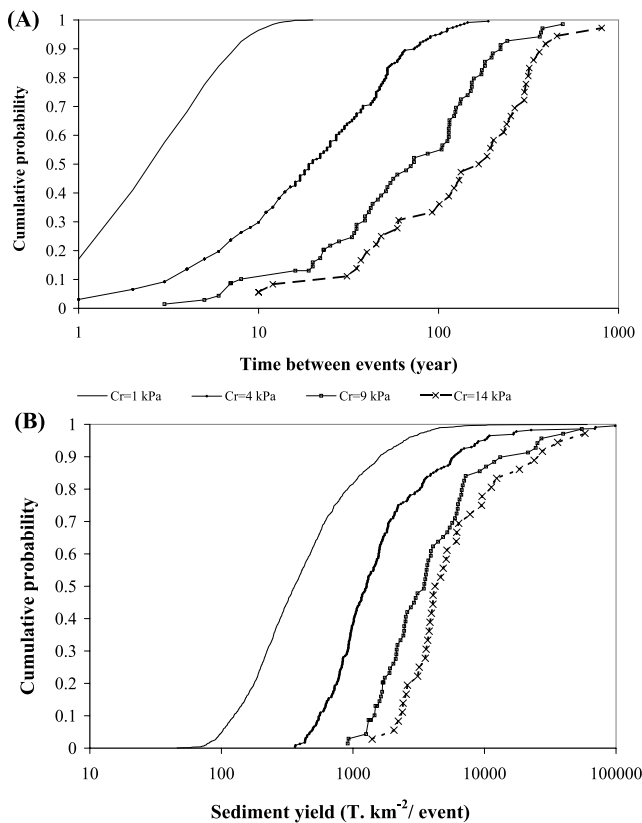
Figure 4. Simulation results for undisturbed forests with progressively increasing root cohesion. (a) Probability distributions of time between events. (b) Probability distribution of sediment yields.

were driven with the same climate and wildfire (only for the wildfire simulations) data. During the 7000 years of the post model spin-up evaluation period the model generated 35 random forest fires, with intervals ranging from 6 to 577 years.

[55] An erosion event is defined as the occurrence of a landslide (FS by equation (18) <1 somewhere in the domain) or overland flow gully erosion when the mean C using mean runoff $\bar{r}$ (equation (7)) is less than the channel initiation threshold $C_F = 500$ m. We plotted the probability distributions of time between erosion events that gives the time available for the stream hydraulic conditions and aquatic communities to recover between subsequent disturbances and the probability distributions of sediment yields to show the natural range of sediment inputs (Figures 4a–4b and 5a–5f). Figure 5 includes the results for both disturbed and undisturbed forest conditions for comparison. We also plotted the probability distributions for the total amount of erosion triggered in the AEP (30 years following the fire) of each simulated fire event. Table 2 presents the mean, 0.05, and 0.95 quantiles of time between events and sediment yields for the simulations.

[56] In the simulations, an increase in root cohesion leads to an increase in the time between erosion events both for undisturbed and episodically disturbed forests with wildfires. This allows soil thickening on hillslopes and promotes an increase in the mean episodic sediment yields (Table 2).
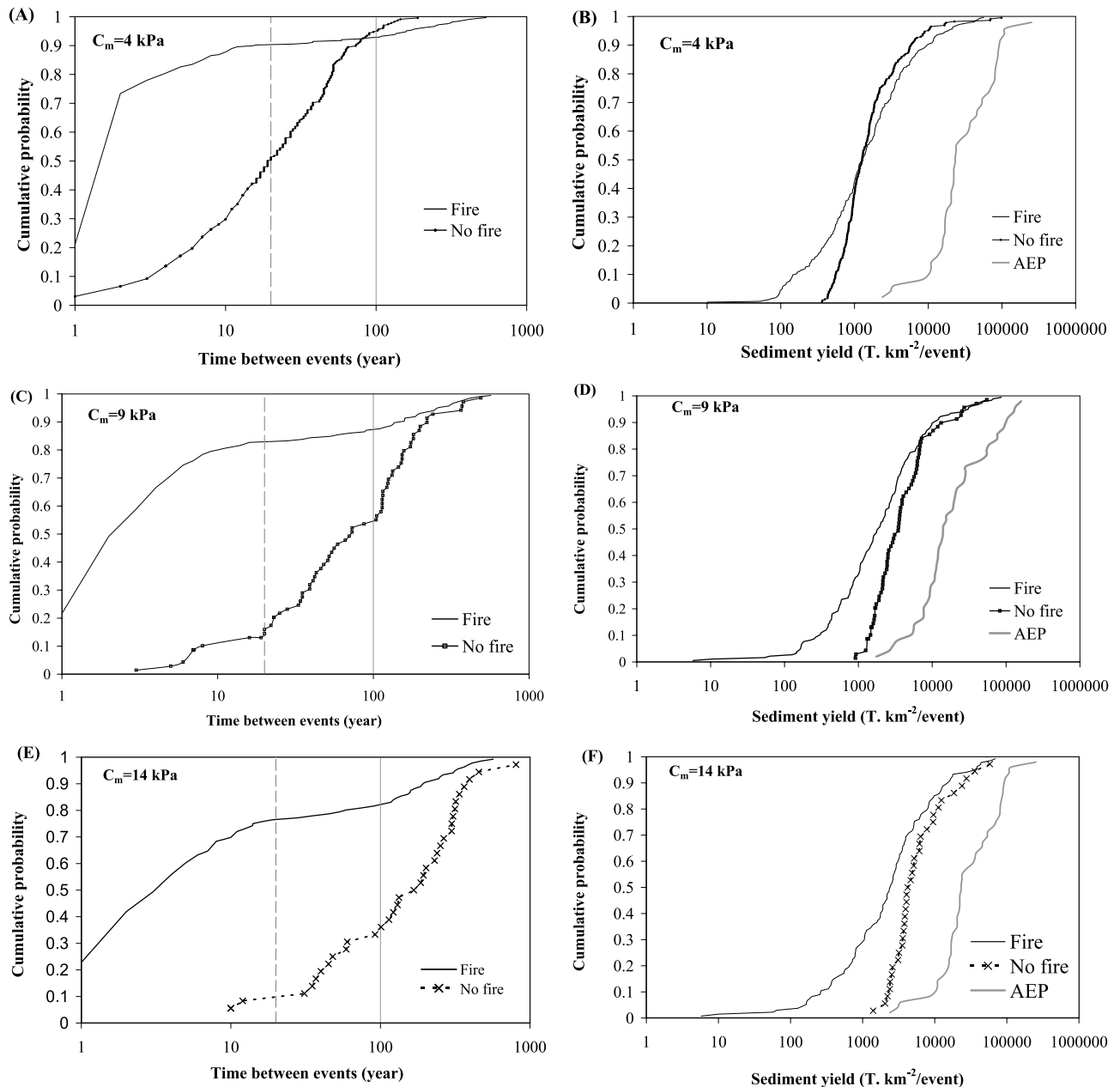
In Figure 4, probability distributions shift to the right as root cohesion increases. The same pattern can be seen for the case of wildfires (Figure 5) because the minimum root cohesion value that would attain following vegetation death would be a fraction of the mature cohesion. The model suggests that individual debris flows triggered due to the thickening of colluvium over thousands of years in undisturbed forests can be more destructive than debris flow triggered more frequently due to fires under the same climate and topographic conditions. This model behavior is consistent with some field observations [*Johnson et al.*, 2000].

[57] In the wildfire simulations, timing of erosion is controlled and synchronized by wildfire. All hollows susceptible to landsliding (i.e., due to thickening of colluvium) are evacuated during the AEPs (first 30 years following the fire before full vegetation recovery). The probability distributions of the time between erosion events for undisturbed and naturally disturbed forests show two distinct patterns (Figure 5). Wildfires caused a 32% decrease in the mean time between erosion events for the case of mature root cohesion 4 kPa and approximately a threefold decrease for the other simulations compared to the undisturbed forest conditions (Table 2). This reduction leads to more frequent erosion events with smaller average magnitudes. In the simulations that include wildfire, on the average, ~82% of the events have time between events ≤20 years (90% for $C_r = 4$ kPa, 82% for $C_r = 9$ kPa, and 76% for $C_r = 14$ kPa).

[58] During the AEPs, there is usually a large event followed by relatively smaller events in the simulations. This behavior causes a longer tail on the probability distribution of sediment yields under wildfire disturbances (Figure 5). In environmental management, not only the individual events but also the total amount of sediment produced by multiple events in the AEPs may be important. It is clear in the plots that total sediment that may enter the streams in the AEPs following fires may be far more than the sediment produced in undisturbed forests in 20–30 years.

[59] AEPs are usually followed by infilling periods that extend until the next fire event. Erosion triggered due to climate forcing is rare between two AEPs. This model behavior can be observed in the probability plots of time between events (Figure 5). The probability curves for all three runs flatten off starting from ~20 to 100 years on the abscissa. This shows that the probability of time between erosion events being between 20 and 100 years is very small. Then, the probability curves steepen slightly after 100 years. In our experiments with the model we found that this second rise in the probability curve corresponds to the time between the last and the first erosion events of two subsequent AEPs following wildfires, recalling that the average recurrence interval between fires is 200 years.

[60] The upslope extent of erosion in the valley network has important implications for the spatial pattern of the vegetation disturbances [*Naiman et al.*, 1998], biodiversity [*Pollok*, 1998], stream temperatures [*Welch et al.*, 1998], and the hydrologic response [*Ziemer and Lisle*, 1998] in forested catchments. Figures 6 and 7 map the areas where episodic sediment scour by debris flows is greater than sediment infilling by diffusion, a criteria that is sometimes suggested to identify the hillslope-valley transition [*Tucker and Bras*, 1998]. This gives the areas subject to net erosion

Figure 5. Probability distribution of sediment yields and time between erosion events under forest fire disturbances for Rocky Mountain douglas fir with mature root cohesion values of (a, b) 4, (c, d) 9, and (e, f) 14 kPa. Vertical lines show the infilling periods where the probability of erosion is very low. AEP, accelerated erosion period.

compared to the initial soil depths imposed at the beginning of the model run. No fluvial erosion is observed in the simulations with constant root cohesion so that the maintenance of the channel network in Figure 6 is solely due to landsliding and debris flow scour [*Dietrich and Dunne*, 1993; *Montgomery and Dietrich*, 1994]. Both Figures 6 and 7 show the stabilizing effects of vegetation. As the value of root cohesion increases, the spatial extent of erosion retreats. In the lowest case of root cohesion (C_r = 1 kPa in Figure 6a), channels extend up to the ridge tops in most locations, and shallow landsliding is observed even in some divergent hillslope positions. The simulation example driven by C_r = 14 kPa shows the other end-member of the

simulations (Figure 6d), where erosion is confined to the valley bottoms and shows discontinuities. Here the discontinuities would occur when scour is rare enough to allow the diffusion processes to evolve soil depths greater than or equal to the initial soil depths. Debris flows are only triggered in the axis of major hollows. In comparing Figures 6 and 7, note also that under the same value of mature root cohesion, wildfires increase the drainage density in the model. Interpretation of these results needs to be tempered by the fact that they were obtained using an existing landform as expressed by the DEM, and over the long term, the different process dominance that determines drainage density is expected to manifest itself in the landform.

Table 2. Simulation Statistics for Different Root Cohesion Values for the Runs With and Without Wildfire Disturbances[a]

	Time Between Events, years			Sediment Yield, t km^{-2} event^{-1}		
Simulation	Mean	$q = 0.05$	$q = 0.95$	Mean	$q = 0.05$	$q = 0.95$
$C_r = 1$ kPa[b]	3.86	1 (0.17)	9	728	101	2400
$C_r = 4$ kPa[b]	30.6	1.8	102	3313	483	10,000
$C_r = 9$ kPa[b]	100	6	371	8162	1258	27,100
$C_r = 12$ kPa[b]	191	10	524	8841	2050	40,300
$C_r = 4$ kPa[c]	21	1 (0.21)	159	3870	104	18,796
$C_r = 9$ kPa[c]	36.7	1 (0.22)	262	5363	164	30,960
$C_r = 12$ kPa[c]	50	1 (0.23)	322	5947	160	36,000

[a]Here q represents quantile. Numbers in parentheses are the minimum cumulative probabilities.
[b]No disturbance.
[c]Wildfire disturbance.

[61] The model results are consistent with field observations that drainage density tends to decrease with increasing vegetation cover or under more humid climates, which promote vegetation [*Gregory*, 1976; *Moglen et al.*, 1998]. When the spatial extent of the simulated erosion patterns in Figure 7 is compared to the contours of the current topography, the extent of the valley network for the case of $C_m = 9$ kPa agrees reasonably well with the converging topographic contour lines. Because the area has been subject to the current fire regime for at least the last 2000 years, this comparison is made using the spatial erosion pattern under the wildfire influence.

4.2. Comparisons With Field Observations

[62] We compared the mean episodic event sediment yields (mean ESY), and the long-term annual averages (LASY) of the simulation (Table 2 and Figure 7 for $C_m = 9$ kPa) with field observations of event sediment yields and short-term and long-term annual average sediment yields (SASY and LASY) measured for several catchments in the Idaho batholith using ^{10}Be [*Kirchner et al.*, 2001] (Figure 8).

[63] We used event sediment yields reported by *Istanbulluoglu et al.* [2003] for the gullies initiated in Trapper Creek due to a thunderstorm event following a wildfire in 1995. We used two debris flow sediment yields reported by *Meyer et al.* [2001], one in a burned and the other in an unburned nonforested site, both triggered in 1997 due to a prolonged rain-on-snow event in the south fork of the Payette River (SFPR) in the Idaho batholith. We also included our observations of a debris flow event that was triggered 8 years after a stand-replacing fire during the same 1997 rain-on-snow event in the SFPR. Sediment yield data for the gullies developed in Trapper Creek and in the SFPR are reported in Figure 8 for cross sections surveyed along gullies. *Meyer et al.* [2001], however, only reports the sediment yield at the basin outlet. SASY and LASY are reproduced from *Kirchner et al.* [2001] for those basins with approximately the same size as the study watershed. SASY observations on the plot represent annual averages of sediment yield over 10–28 years of observations from sediment traps and gauges, whereas the LASY represent the averages over ~10,000 years deduced from ^{10}Be of sediments.

[64] Field data reported for event sediment yields are bounded between the 8% and 95% quantiles of the simulated event sediment yields. Most of the observations are between the mean and 95% quantile. We recognize that this comparison is weak because the observations we use are only from recent catastrophic erosion events in the region, but nevertheless Figure 8 shows that the model is capable of producing extreme event sediment yields that are observed in the region. The long-term average sediment yield predicted by the model is 141 t km^{-2} yr^{-1} in 7000 years. Since
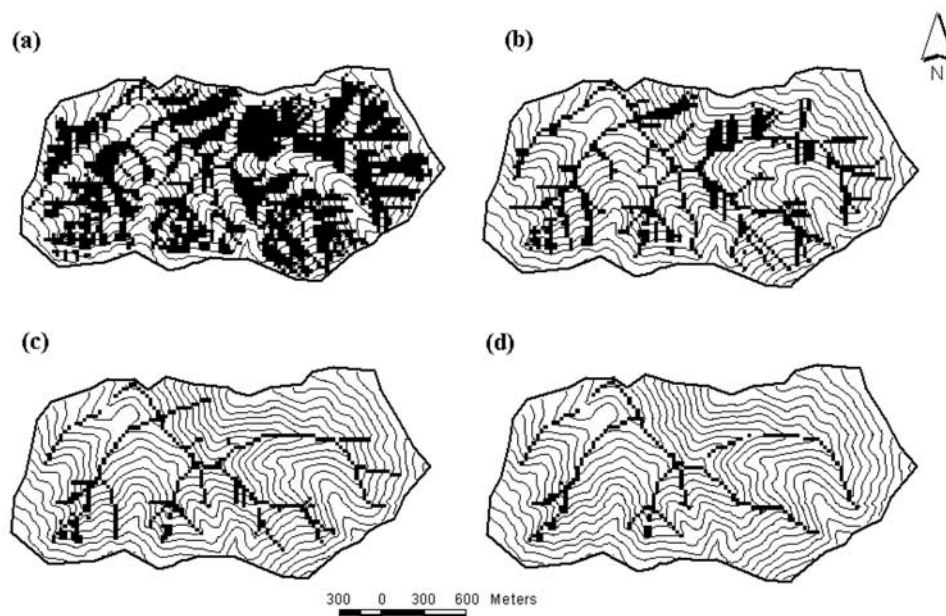

Figure 6. Channel network predicted where sediment scour by debris flows is higher than the amount of sediment infilling by diffusive processes (net erosion) over the long term for undisturbed conditions: (a) $C_r = 1$ kPa; (b) $C_r = 4$ kPa; (c) $C_r = 9$ kPa; and (d) $C_r = 14$ kPa.
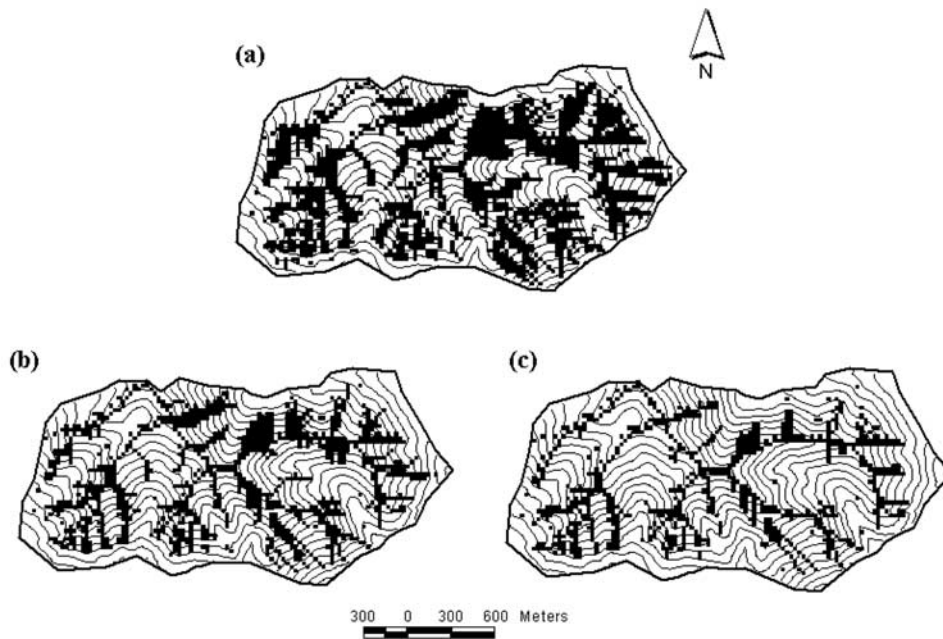
Figure 7. Channel network predicted where sediment scour is higher than sediment infilling by diffusive processes (net erosion) over the long term with wildfire disturbances. Simulated impact of mature root cohesion (a) $C_m = 4$ kPa, (b) $C_m = 9$ kPa, and (c) $C_m = 14$ kPa.

the model is not developed to simulate the day-to-day incremental erosion, this average only includes the episodic events. The SASY reported by *Kirchner et al.* [2001] did not include any episodic events and has an average value of ~ 12 t km^{-2} yr^{-1} (average of 19 watersheds). When we add this SASY to the long-term averages of episodic events that

the model predicts, we find 153 t km^{-2} yr^{-1} for the LASY. Modeled LASY is plotted in Figure 8 and shows good correspondence with the observed long-term averages. We found that on average, episodic sediment delivery of an erosion event is between 35 and up to 560 times greater than the long-term averages. When compared to the short-term
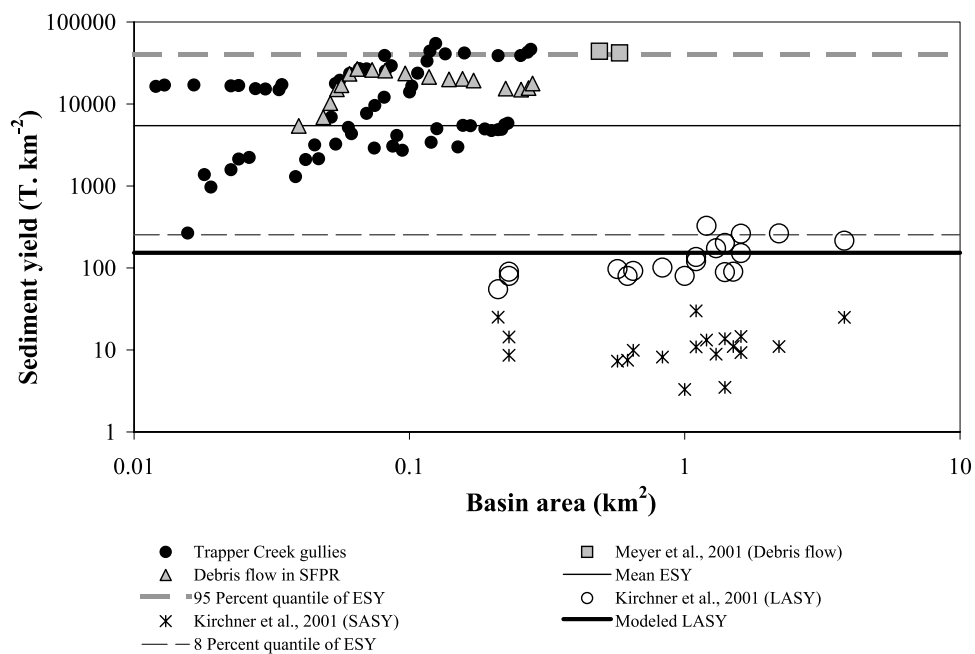
Figure 8. Comparisons of the mean and the 8% and 95% quantile of event sediment yields (ESY) and long-term averages (LASY) of 7000 years of simulation using the mature root cohesion value of 9 kPa, with the observed event and short-term (10–28 years) average sediment yields (SASY) and the long-term ($\sim 10,000$ years) average sediment yields obtained using cosmogenic ^{10}Be.
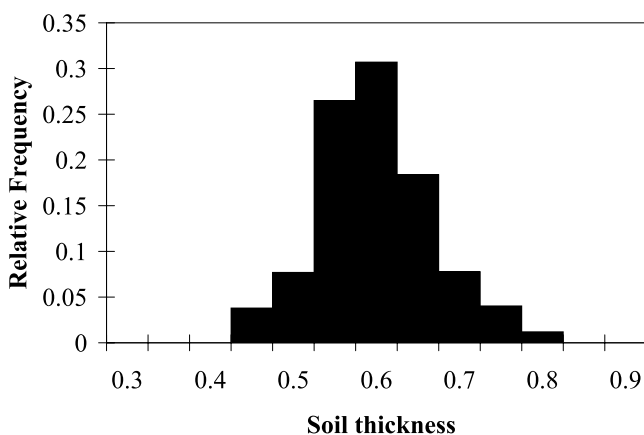
sediment yields, we found that the episodic yields are, on average, 450 and up to 7200 times greater. These results suggest that under natural disturbances, ~92% of the sediment delivery is due to low-frequency and high-magnitude erosion events in the region.

[65] On the basis of the probability distribution of sediment yields reported here, one can approximate the return interval (1 divided by the exceedance probability) of major catastrophic events recently observed in the area. Event sediment yields reported by *Meyer et al.* [2001] and the upper bound of the rates reported by *Istanbulluoglu et al.* [2003] are ~40,000 t km^{-2}. The model predicts a probability of 0.05 (95% quantile) for events of this magnitude or higher. For the simulation reported in Figure 8, our results give a probability of a year with an episodic event as 1/36. Multiplying these two probabilities gives a probability of an episodic event of 40,000 t km^{-2} around ~0.0014, and this corresponds to a return period of 1 in ~700 years.

4.3. Timber Harvest

[66] How do anthropogenic vegetation disturbances caused by forest management occurring over relatively short timescales affect the episodic behavior of sediment yields? In this section we designed a numerical paired watershed experiment, where we compared the effects of clear-cutting (anthropogenic) and wildfire (natural) disturbances on sediment yields.

[67] Clear-cutting is the easiest and the least expensive timber harvest technique, often preferred by land managers because of its simplicity [*Sidle et al.*, 1985]. In a more detailed study, one could add conservation practices such as buffer strips and partial cutting, thinning, and shelterwood in models. However, because of the uncertainties associated with the other management techniques in terms of their influence on the temporal and spatial variation of root cohesion [*Schmidt et al.*, 2002], parameterization of such a modeling study would be difficult with the current level of understanding. Therefore our study should be considered as

Table 3. Comparison of the Average Simulated Sediment Yields and the Number of Erosion Events Under Anthropogenic (Harvest) and Natural (Wildfire) Disturbance Regimes for Three Different Soil Depth Initial Conditions
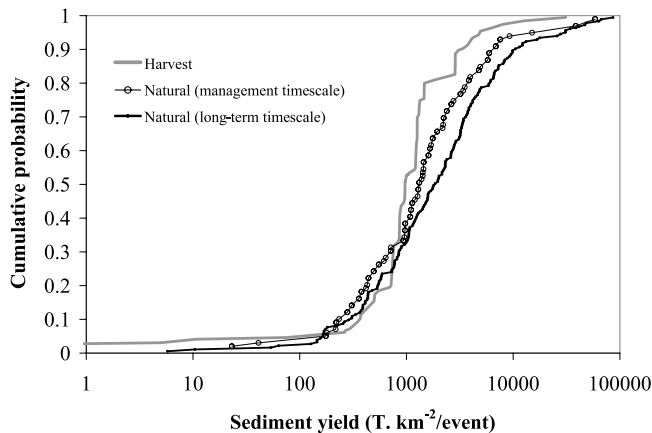
Initial Condition	Harvest		Natural	
	Erosion Events	Sediment Yields, t km^{-2} yr^{-1}	Erosion Events	Sediment Yields, t km^{-2} yr^{-1}
Minimum	38	26	34	46
Average	194	67	98	74
Maximum	327	235	126	145

a simple thought experiment as an initial step to more detailed modeling studies.

[68] We showed in the previous simulations that under the recent natural disturbance regime and dominant vegetation cover, natural fire disturbances along with stochastic climate events alter the soil depths and the magnitude of sediment yields in time. The severity of erosion following vegetation removal may be influenced by the initial condition of colluvium thicknesses in the basin. This is often ignored in forest management. We obtained a minimum, average, and maximum initial condition for spatial soil depths from the long-term simulation (7000 years) reported in Figure 8, assuming that this simulation would represent the natural variation in soil depths and sediment yields. In this simulation, the spatial average of the soil depths varies between 0.4 and 0.77 m, with a mean, standard deviation, and skewness of 0.57, 0.068, and 0.26 m, respectively. Figure 9 shows the histogram of these possible initial soil depth conditions. Basin-averaged soil depths are greater than or equal to the mean value of 0.57 m 60% of the time in the simulation.

[69] The rotation age for timber harvest is between 80 and 120 years in the Idaho batholith for healthy and unburned forests [*U.S. Department of Agriculture Forest Service*, 1990]. In the model we used 100 years for rotation length and modeled three rotations where all the vegetation is removed for each soil depth initial condition. We assumed that no wildfires ignite during the management period. For the control case, however, we modeled forest fires based on the fire probability of $P_F = 0.005$ (mean return period of 200 years) during the comparison period of 300 years. The same random climate events are used in both cases, and the experiment is repeated 21 times, in other words, 21 different climate event and fire occurrence sequences for a total of 6300 years with 63 clear-cuts.

[70] We recorded the number of erosion events triggered during the repeated simulations and calculated the average sediment yields for all three model initial conditions both for harvest and natural disturbances (Table 3). Since our model only accounts for episodic sediment delivery, we added a background rate of 12 t km^2 yr^{-1} [*Kirchner et al.*, 2001] to the average sediment yields in order to make the model predictions comparable with the long-term average sediment yields reported by *Kirchner et al.* [2001]. Figure 10 plots the probability distributions of the simulated episodic event sediment yields for both harvest and natural disturbances in the 300 year management timescale using the average soil depth initial condition and the distribution for the long-term episodic sediment yields under wildfire

Figure 9. Histogram of the basin-averaged soil depth in 7000 years of the long-term simulation under the natural fire regime (mature root cohesion is 9 kPa). Note that the probability distribution of sediment yields and time between erosion events was reported for this simulation in Figures 5c and 5d and that sediment yields were compared with field observations in Figure 8.

Figure 10. Probability distributions of event sediment yields under harvest and natural (fire) disturbances during the management timescale for the initial condition, with average soil depth, and long-term sediment yields that represent the natural sediment yield regime in the region. In these simulations the mean event sediment yield is 1814 t km^{-2} for the harvest, 3964 t km^{-2} for the natural disturbances over the management timescale, and 5363 t km^{-2} for natural disturbances over the long-term timescale.

disturbances using the mature root cohesion value of 9 kPa. The latter distribution, already presented in Figure 5, is included here for comparison purposes with the management-scale variations in sediment yields and to further see if the idea of comparing short-term average sediment yields to long-term averages is a plausible practice to develop land use strategies to control erosion. Statistics of the probability distributions in Figure 10 are reported in Table 4.

[71] Our results (Table 3) show that initial sediment availability on hillslopes when forest management is started has a large influence on the erosion rates. Under the harvest prescription, there is a factor 9 difference between the number of erosion events and average sediment yields over the range from minimum to maximum initial soil depth. Under natural (wildfire disturbance) conditions the differences in initial soil depth result in up to a factor 3.7 difference in the number of erosion events and average sediment yields from minimum to maximum initial soil depth. Annual sediment yield for the shallow initial condition is less in harvested areas than in natural areas. However, it is about equal for the average soil depth initial condition. Annual sediment yield is significantly greater in harvested areas than in natural areas for deep soils. This also implies that soil depth has an important control on the relative effects of harvest and fire.

[72] Comparison between the harvest and natural disturbances shows that, on the average, harvesting doubled the number of erosion events (Table 3). This is because of the regularity of the harvest disturbances in every 100 years compared to fire disturbances that are probabilistic with a return interval of 200 years in the region.

[73] The mean and standard deviation of event sediment yields are higher under natural disturbances, both over the management and long-term timescales, than event sediment yields under harvest prescription. However, it is also important to note that the 7th through 30th percentile event

sediment yields for the management timescale and 26th percentile for the long-term are all lower for the natural condition than for the harvested condition. The primary reason for the shift in the mean is that there is a greater variance under natural conditions, which implies additional sources of variability. Gully erosion under natural conditions due to fire-induced water repellence is one additional process that is not likely to occur under harvest conditions. In addition to this, a greater variation in root strength at the time of failure is likely in natural conditions because of the random arrival of fires with a mean of 200 years. The harvest scenarios with a rotation of 100 years produce a greater amount of time spent at low root strengths, increasing vulnerability to loss under lesser climatic events that leads to more frequent low-magnitude (due to lesser soil accumulation in hollows) erosion events.

[74] Figure 10 and Table 4 report higher event sediment yields during the long-term timescale (7000 years) than during the short (management) time frame. This is because the spatial configuration of soil depths that is produced during long-term simulations was not fully reproduced during the short-term experiments. For example, for the case of wildfire simulations the erosion response to fires that started close to the end of a 300 year management period or to back-to-back fires were not successfully modeled because of a 300 year truncation applied for comparison with harvest cycles. In some cases the model did not even produce any fires during this period. We suggest that comparing sediment yields measured or simulated in relatively short time-scales with the long-term averages for decision making in forest management may underestimate the consequences of forest management and may not even be a valid criteria, especially when not only the magnitude but also the frequency of disturbances is important (i.e., for aquatic habitats).

5. Conclusions

[75] We have presented a detailed model for the episodic behavior of sediment delivery in steep-forested headwater catchments and the factors that contribute to its variability. Verification of a comprehensive model over long timescales is difficult due to the scarcity of measurements. Nevertheless, we used the information available to verify the model to the extent possible. The model was then used to address questions of how sediment yields respond to various disturbances, both natural and anthropogenic. A key result

Table 4. Mean, Standard Deviation, Skewness, 5% and 95% Quantiles, q, of the Event Sediment Yields Over the Simulated 300 Year Management Period for the Harvest (100 Year Cycle) Prescription and Natural Disturbances (Wildfires) With Average Soil Depth Initial Condition and for the Long-Term (7000 Year) Simulations

Statistical Parameter	Sediment Yield, t km^{-2} event^{-1}		
	Harvest	Natural	Long Term
Mean	1814	3964	5363
Standard deviation	3466	9749	11,640
Skewness	6.74	4.62	4.34
$q = 0.05$	110	175	164
$q = 0.95$	4900	15,048	30,960

is that the model was able to reproduce both long-term erosion rates and episodic event sediment yields that have been reported in the literature. This literature had suggested that long-term sediment production was dominated by infrequent episodic events, and the model provided a quantitative framework that reconciled the observed mismatch of several orders of magnitude between short-term (on the order of decades) and long-term ($\sim$10,000 years) sediment yields.

[76] In addressing the questions of how forest stand density and disturbance influence sediment yields, a key finding was that long-term sediment delivery is dominated by episodic events that evacuate essentially all sediment from hollows subject to erosion and landsliding. The threshold for these evacuation events is controlled by vegetation root cohesion and density. Root cohesion exerts control over the landsliding and is dictated by decay and recovery following disturbance. Vegetation density exerts control over roughness, which plays a role in surface erosion. Surface erosion is also influenced by water repellency following fire. These effects all combine to result in the occurrence of episodic evacuation events being associated with a period of accelerated erosion (AEP) following disturbance. However, the magnitude of these episodic events was found to be controlled by the buildup of soil in the hollows subject to erosion and landsliding. This soil buildup is dictated by the slope-dependent hillslope transport flux and soil production function, both of which are constant rates in the model. Therefore the magnitude of episodic sediment production events was found to be inversely proportional to their frequency.

[77] Our simulation results showed good correspondence with the field observations of both catastrophic sediment yields and long-term averages. The model results suggest that in a typical steep-forested basin in the Idaho batholith, 92% of the sediment delivery is due to infrequent episodic events under the current climate and wildfire regime. We used our simulation results to estimate the return period for some recent catastrophic debris flow events observed in Idaho that delivered approximately 40,000 t km^{-2} of sediment per event. We estimated a return period of 1 in 700 years for these events. This is useful to ecologists given the importance of the recurrence interval of major channel-reorganizing events on aquatic habitats [*Reeves et al.*, 1998].

[78] The model emphasizes the importance of vegetation and vegetation disturbances due to wildfires on the episodic nature of sediment yields. In the absence of disturbances, sediment delivery is modeled to be less frequent but with higher magnitudes. In these cases, timing of mass failure is controlled by the time required to accumulate a critical depth of colluvium that increases as a function of cohesion under a stochastic climate forcing. Thus an increase in root cohesion also decreases the frequency of sediment yields. Our model suggests that forest fires control the timing of sediment delivery. We find that all else being equal, introducing the current wildfire regime in the model decreases the mean time between erosion events up to threefold and leads to more frequent erosion events with smaller average magnitudes manifested with a longer tail in the probability distribution of sediment yields. An important finding in the episodic behavior of the sediment yields under forest fire

conditions is the emergence of accelerated erosion periods, here defined as the first 30 year time window following a wildfire where erosion thresholds imposed by vegetation are low. AEPs have the effect of synchronizing the sediment yields from different parts of the watershed to occur in the years immediately following a fire before vegetation recovery. Therefore during these times the total sediment yields summed over the AEP significantly exceeds the yields under no disturbance conditions. One interesting outcome of the model is that in the period between two AEPs, a climate-driven geomorphic response is less likely. This has implications for simple climate threshold models that postulate a one to one correspondence between the climate state and geomorphic response. Modeling the geomorphic response to climate inputs needs to account for the history of inputs and time required for the accumulation of material that can be episodically evacuated.

[79] Earlier modeling work [i.e., *Dietrich et al.*, 1993; *Tucker and Slingerland*, 1997] suggested that in fluvial systems, drainage density is controlled by an erosion threshold due to vegetation cover that limits soil incision due to running water [*Prosser*, 1996; *Prosser and Soufi*, 1998]. Thus a decrease in erosion thresholds due to, for example, vegetation destruction would lead to expansion of the fluvial channel erosion onto diffusion-dominated hillslopes. Our model runs underscore forest vegetation as an important factor that controls drainage density both in debris flow-dominated environments in the absence of fluvial erosion (Figure 6) and in areas where both fluvial erosion and debris flows are observed following wildfires (Figure 7). Our results suggest that all else being equal, wildfires may increase the drainage density significantly. This can be observed by comparing Figures 6d and 7c.

[80] In comparing sediment yields under harvest and wildfire disturbances, we find a factor of 9 difference between the number of erosion events and average sediment yields over the range from minimum to maximum initial soil depth. Harvest disturbances double the number of erosion events in the area per unit time. In considering shorter-term consequences of harvesting management options over a 300 year management period, we found that the sediment production depends upon the average soil depth initial conditions, which are, at present, unknown. If soil depth is above average, then the introduction of harvest cycles will increase stream sediment inputs over this management period. If, on the other hand, soil depth is less than average, then sediment production following the introduction of harvest cycles is likely to be less than the long-term average. We found that there is a 60% chance that harvest prescription would increase the average sediment yields as in the long-term simulations, the spatial average of the soil depths is greater than or equal to their time average 60% of the time (Figure 9). As the number of erosion events is higher under harvest prescription than under natural conditions in our simulations, we may expect, on the average, larger event sediment yields under natural conditions. However, the important finding here for land management is not the amount of sediment delivery but the increased frequency of stream disturbances that is believed to be an important factor in habitat fragmentation [*Dunham et al.*, 1997].

[81] Our findings in this paper underscore the difficulty in making land use decisions based on the comparison of

short-term sediment yields in basins with different land cover conditions and wildfire and erosion histories. A longer-term perspective that considers the episodic history of sediment production and how this is changed by management needs to be taken.

[82] In this paper we modeled the interactions between forest vegetation and vegetation disturbances with the timing and magnitude of sediment yields that disturb aquatic habitats. We feel that this is only one aspect of the problem. Remaining related questions to explore are (1) How would the aquatic ecosystem evolved to cope with a natural regime of disturbances respond to changes in the disturbance regime? and (2) How may we manage forests without causing significant alterations to the biologic and aquatic ecosystems?

[83] Future model developments in forest management require the merging of two research directions. One is continuing to understand the physical basis of hydrologic and geomorphic response and developing state of the art erosion and landscape evolution theories. The second is to develop quantitative theories for the evolution of ecosystems under disturbances.

Notation

$\bar{P}$ mean summer rainfall depth.
$\bar{D}$ mean summer rainfall duration.
$\overline{wi}$ mean winter water input rate.
SD   snow depth.
RSW   ratio of snow density to the density of water.
r instantaneous runoff rate.
p instantaneous rainfall rate.
I_c infiltration capacity.
$\bar{p}$ average rainfall rate.
η impervious watershed fraction.
$f(\ )$ probability density function.
z elevation.
h_s soil thickness perpendicular to slope.
ρ_r, ρ_s rock and soil bulk density, respectively.
s ratio of sediment to water density.
C threshold for channel initiation.
d_{50} median sediment size for hillslope surface material.
a unit contributing area.
A drainage area.
R_w relative wetness.
S slope.
PCI   probability of channel initiation.
f_s shear stress partitioning ratio.
n_s Manning's roughness coefficient for bare soil.
n_V Manning's roughness coefficient for vegetation.
τ_f effective shear stress of concentrated flow.
τ_* nondimensional shear stress.
τ_c critical shear stress.
τ_{fo} effective shear stress for overland flow.
K   diffusion constant.
K_s saturated hydraulic conductivity.
d median sediment size for sediment transport.
q_s unit sediment discharge.
W_f flow width.
γ sediment transport coefficient.
κ calibration constant.

p_f shear stress exponent.
m discharge per unit area exponent, shear stress equation.
n slope exponent, shear stress equation.
M area exponent, sediment transport equation.
N slope exponent, sediment transport equation.
χ_w constant that relates discharge and slope to flow width.
χ_τ constant that relates discharge and slope to flow shear stress.
FS   factor of safety.
C_r root cohesion.
C_s soil cohesion.
C_m mature root cohesion.
θ ground slope angle.
n_v^m overland flow roughness for mature forest.
D_r rate of root cohesion decay.
R_r rate of root cohesion recovery.
k_C, n_C root strength parameters for decay.
a_C, b_C root strength parameters for regrowth.
c_C, ξ_C root strength parameters for regrowth, continued.
ϕ soil internal friction angle.
P_f watershed pervious fraction.
F_{gc} fractional ground cover.
k_B biomass growth on a bare surface.
B_c plant related constant.
P_F probability of wildfire.

References

Alberts, E. E., M. A. Weltz, and F. Ghidey (1989), Plant growth component, in *USDA—Water Erosion Prediction Project: Hillslope Profile Model Documentation*, edited by L. J. Lane and M. A. Nearing, *NSERL Rep. 2*, pp. 8.1–8.38, Nat. Soil Erosion Res. Lab., West Lafayette, Ind.

Anderson, R. S. (2002), Modeling the tor-dotted crests, bedrock edges, and parabolic profile of high alpine surfaces of the Wind River Range, Wyoming, *Geomorphology*, *46*, 35–58.

Arcement, G. J. J., and V. R. Schneider (1984), Guide for selecting Manning's roughness coefficients for natural channels and floodplains, *Rep. RHWA-TS-84-204*, 50 pp., U.S. Geol. Surv., Reston, Va.

Arnold, J. G., M. A. Weltz, E. E. Alberts, and D. C. Flanagan (1995), Plant growth component, in *USDA—Water Erosion Prediction Project*, *Rep. 10*, chap. 8, pp. 8.1–8.41, Nat. Soil Erosion Res. Lab., West Lafayette, Ind.

Barret, S., S. Arno, and J. Menakis (1997), Fire episodes in the inland northwest (1540–1940) based on fire history data, *Rep. INT-GTR-370*, Intermt. For. and Range Exp. Stn., Ogden, Utah.

Benavides-Solorio, J., and L. H. MacDonald (2001), Post-fire runoff and erosion from simulated rainfall on small plots, Colorado Front Range, *Hydrol. Processes*, *15*, 2931–2952.

Benda, L. E., and T. W. Cundy (1990), Predicting deposition of debris flows in mountain channels, *Can. Geotech. J.*, *27*, 409–417.

Benda, L., and T. Dunne (1997a), Stochastic forcing of sediment supply to channel networks from landsliding and debris flow, *Water Resour. Res.*, *33*(12), 2849–2863.

Benda, L., and T. Dunne (1997b), Stochastic forcing of sediment routing and storage in channel networks, *Water Resour. Res.*, *33*(12), 2865–2880.

Benda, L., D. J. Miller, T. Dunne, and G. H. Reeves (1998), Dynamic landscape systems, in *River Ecology and Management: Lessons From*

the Pacific Coastal Ecoregion, edited by R. J. Naiman and R. E. Bilby, pp. 261–288, Springer-Verlag, New York.

Benjamin, J. R., and C. A. Cornell (1970), Probability, Statistics, and Decision for Civil Engineering, 684 pp., McGraw-Hill, New York.

Burroughs, E. R., and B. R. Thomas (1977), Declining root strength in Douglas-fir after felling as a factor in slope stability, USDA For. Serv. Res. Pap. INT-190, 27 pp., Intermt. For. and Range Exp. Stn., Ogden, Utah.

Cannon, S. H., P. S. Powers, and W. Z. Savage (1998), Fire-related hyperconcentrated and debris flows on Storm King Mountain, Glenwood Springs, Colorado, Environ. Geol., 35, 210–218.

Cannon, S. H., E. R. Bigio, and E. Mine (2001), A process for fire-related debris flow initiation, Cerro Grande fire, New Mexico, Hydrol. Processes, 15, 3011–3023.

Chow, V. T. (1959), Open Channel Hydraulics, McGraw-Hill, New York.

Clayton, J. L., and W. F. Megahan (1986), Erosional and chemical denudation rates in the Idaho Batholith, Earth Surf. Processes Landforms, 11, 389–400.

Clayton, J. L., and W. F. Megahan (1997), Natural erosion rates and their prediction in the Idaho Batholith, J. Am. Water Resour. Assoc., 33(3), 689–703.

Clayton, J. L., W. F. Megahan, and D. Hampton (1979), Soil and bedrock properties: Weathering and alteration products and processes in the Idaho Batholith, USDA For. Serv. Res. Note INT-237, 35 pp., Intermt. For. and Range Exp. Stn., Ogden, Utah.

Cox, N. J. (1980), On the relationship between bedrock lowering and regolith thickness, Earth Surf. Processes Landforms, 5, 271–274.

Crozier, M. J. (1981), Landslides Causes, Consequences, and Environment, Croom Helm, London.

DeBano, L. F. (1981), Water repellent soils: A state-of-the-art, Tech. Rep. PSW-46, U.S. Dep. of Agric. For. Serv. Gen., Washington, D. C.

Dietrich, W. E., and T. Dunne (1993), The channel head, in Channel Network Hydrology, edited by K. Beven and M. J. Kirkby, pp. 175–219, John Wiley, Hoboken, N. J.

Dietrich, W. E., C. J. Wilson, and S. L. Reneau (1986), Hollows, colluvium and landslides in soil mantled landscapes, in Hillslope Processes, edited by A. D. Abrahams, pp. 361–388, Allen and Unwin, Concord, Mass.

Dietrich, W. E., C. J. Wilson, and D. R. Montgomery (1993), Analysis of erosion thresholds, channel networks, and landscape morphology using a digital terrain model, J. Geol., 101, 259–278.

Dietrich, W. E., R. Reiss, M.-L. Hsu, and D. R. Montgomery (1995), A process-based model for colluvial soil depth and shallow landsliding using digital elevation data, Hydrol. Processes, 9, 383–400.

Dietrich, W. E., D. Bellugi, and R. R. D. Asua (2000), Validation of the shallow landslide model, SHALSTAB, for forest management, in Land Use and Watersheds: Human Influence on Hydrology and Geomorphology in Urban and Forest Areas, Water Sci. Appl. Ser., vol. 2, edited by M. S. Wigmosta and S. J. Burges, pp. 195–227, AGU, Washington, D. C.

Dunham, J. B., G. L. Vinyard, and B. E. Rieman (1997), Habitat fragmentation and extinction risk of Lahontan cutthroat trout, N. Am. J. Fish. Manage., 17, 1126–1133.

Eagleson, P. S. (1978), Climate, soil and vegetation: 2. The distribution of annual precipitation derived from observed storm sequences, Water Resour. Res., 14(5), 713–721.

Engman, E. T. (1986), Roughness coefficients for routing surface runoff, J. Irrig. Drain. Eng., 112(1), 39–53.

Foster, G. R. (1982), Modeling the erosion process, in Hydrologic Modeling of Small Watersheds, ASAE Monogr., vol. 5, edited by C. T. Haan, pp. 295–380, Am. Soc. Agric. Eng., St. Joseph, Miss.

Freeman, G. E., W. J. Rahmeyer, and R. R. Copelan (2000), Determination of resistance due to shrubs and woody vegetation, Rep. ERDC/CHL TR-00-25, 62 pp., U.S. Army Corps of Eng., Washington, D. C.

Garde, R. J., and K. G. R. Raju (1985), Mechanics of Sediment Transportation and Alluvial Stream Problems, 2nd ed., 618 pp., John Wiley, Hoboken, N. J.

Gray, D. H., and W. F. Megahan (1981), Forest vegetation removal and slope stability in the Idaho Batholith, USDA For. Serv. Res. Pap. INT-271, 23 pp., Intermt. For. and Range. Exp. Stn., Ogden, Utah.

Gregory, K. J. (1976), Drainage networks and climate, in Geomorphology and Climate, edited by E. Derbyshire, pp. 289–315, Wiley-Interscience, Hoboken, N. J.

Hampton, D., W. F. Megahan, and J. L. Clayton (1974), Soil and rock properties research in the Idaho Batholith, 126 pp., Dept. Civ. Eng. Howard Univ., Washington, D. C.

Heimsath, A. M., W. E. Dietrich, K. Nishlizumi, and R. C. Finkel (1997), The soil production function and landscape equilibrium, Nature, 388(24), 358–361.

Heimsath, A., W. E. Dietrich, K. Nishiizumi, and R. C. Finkel (2001), Stochastic processes of soil production and transport: Erosion rates, topo-

graphic variation and cosmogenic nuclides in the Oregon Coast Range, Earth Surf. Processes Landforms, 26, 531–552.

Huggins, L. F., and J. R. Burney (1982), Surface runoff, storage and routing, in Hydrologic Modeling of Small Watersheds, edited by C. T. Haan, pp. 169–225, Am. Soc. Agric. Eng., St. Joseph, Mich.

Hutchinson, M. F. (1995), Stochastic space-time weather models from ground-based data, Agric. For. Meteorol., 73, 237–264.

Iida, T. (1999), A stochastic hydro-geomorghological model for shallow landsliding due to rainstorm, Catena, 34, 293–313.

Istanbulluoglu, E., D. G. Tarboton, R. T. Pack, and C. Luce (2002), A probabilistic approach for channel initiation, Water Resour. Res., 38(12), 1325, doi:10.1029/2001WR000782.

Istanbulluoglu, E., D. G. Tarboton, R. T. Pack, and C. Luce (2003), A sediment transport model for incision of gullies on steep topography, Water Resour. Res., 39(4), 1103, doi:10.1029/2002WR001467.

Johnson, A. C., D. N. Swanston, and K. E. McGee (2000), Landslide initiation, runout and deposition within clearcuts and old-growth forests of Alaska, J. Am. Water Resour. Assoc., 36(1), 17–30.

Julien, P. Y., and D. B. Simons (1985), Sediment transport capacity of overland flow, Trans. Am. Soc. Agric. Eng., 28(3), 755–762.

Karsian, E. A. (1995), A 6800-year vegetation and fire history in the Bitterroot Range, Montana, M. S. thesis, Univ. of Mont., Bozeman.

Kidd, W. J. J. (1964), Probable return periods of rainstorms in central Idaho, U.S. Dep. Agric. For. Serv. Res. Note INT-28, 8 pp., Intermt. For. and Range Exp. Stn., Ogden, Utah.

Kirchner, J. W., R. C. Finkel, C. S. Riebe, D. E. Granger, J. L. Clayton, J. G. King, and W. F. Megahan (2001), Mountain erosion over 10 yr, 10 k. y., and 10 m. y. time scales, Geology, 29, 591–594.

Lancaster, S. T., S. K. Hayes, and G. E. Grant (2003), Effects of wood on debris flow runout in small mountain watersheds, Water Resour. Res., 39(6), 1168, doi:10.1029/2001WR001227.

Megahan, W. F. (1978), Erosion processes on steep granitic road fills in central Idaho, Soil Sci. Soc. Am. J., 42(2), 350–357.

Megahan, W. F. (1983), Hydrologic effects of clearcutting and wildfire on steep granitic slopes in Idaho, Water Resour. Res., 19(3), 811–819.

Megahan, W. F. (1992), An overview of erosion and sedimentation processes on granitic soils, in Decomposed Granitic Soils, pp. 11–30, Univ. of Calif., Davis.

Megahan, W. F., and D. C. Molitor (1975), Erosional effects of wildfire and logging in Idaho, in Watershed Management Symposium, pp. 423–444, Am. Soc. Chem. Eng. Irrig. and Drain. Div., Logan, Utah.

Megahan, W. F., N. F. Day, and T. M. Bliss (1978), Landslide occurrence in the western and central northern Rocky Mountain physiographic province in Idaho, in Fifth North American Forest Soils Conference, edited by C. T. Youngberg, pp. 116–139, Colo. State Univ., Ford Collins.

Megahan, W. F., K. A. Seyedbagheri, and P. C. Dodson (1983), Long-term erosion on granitic roadcuts based on exposed tree roots, Earth Surf. Processes Landforms, 8, 19–28.

Meyer, G. A., and S. G. Wells (1997), Fire-related sedimentation events on alluvial fans, Yellowstone National Park, USA, J. Sediment. Res., 67(5), 776–791.

Meyer, G. A., J. L. Pierce, S. H. Wood, and A. J. T. Jull (2001), Fire, storms and erosional events in the Idaho Batholith, Hydrol. Processes, 15, 3025–3038.

Moglen, G. E., E. A. B. Eltahir, and R. L. Bras (1998), On the sensitivity of drainage density to climate change, Water Resour. Res., 34(4), 855–862.

Montgomery, D. R., and W. E. Dietrich (1994), A physically based model for the topographic control on shallow landsliding, Water Resour. Res., 30(4), 1153–1171.

Montgomery, D. R., K. M. Schmidt, H. M. Greenberg, and W. E. Dietrich (2000), Forest clearing and regional landsliding, Geology, 28, 311–314.

Montgomery, D. R., W. E. Dietrich, and J. T. Heffner (2002), Piezometric response in shallow bedrock at CB1: Implications for runoff generation and landsliding, Water Resour. Res., 38(12), 1274, doi:10.1029/2002WR001429.

Moody, J. A., and D. A. Martin (2001), Initial hydrologic and geomorphic response following a wildfire in the Colorado front range, Earth Surf. Processes Landforms, 26, 1049–1070.

Moore, I. D., G. J. Burch, and P. J. Wallbrink (1986), Preferential flow and hydraulic conductivity of forest soils, Soil Sci. Am. J., 50, 876–881.

Naiman, R. J., K. L. Fetcherston, S. J. McKay, and J. Chen (1998), Riparian forests, in River Ecology and Management: Lessons From the Pacific Coastal Ecoregion, edited by R. J. Naiman, R. E. Bilby, pp. 289–323, Springer-Verlag, New York.

Nielsen, D. R., J. W. Biggar, and K. T. Erh (1973), Spatial variability of field-measured soil-water properties, Hilgardia, 42, 215–260.

Pack, R. T., D. G. Tarboton, and C. N. Goodwin (1998), Terrain stability mapping with SINMAP, technical description and users guide for version 1.00, Rep. 4114-0, Terratech Consulting, Salmon Arm, B. C., Canada.

Pollok, M. M. (1998), Biodiversity, in *River Ecology and Management: Lessons From the Pacific Coastal Ecoregion*, edited by R. J. Naiman and R. E. Bilby, pp. 430–452, Springer-Verlag, New York.

Prosser, I. P. (1996), Thresholds for channel initiation in historical and Holocene times, southeastern Australia, in *Advances in Hillslope Processes*, edited by M. G. Anderson and S. M. Brooks, pp. 687–708, John Wiley, Hoboken, N. J.

Prosser, I. P., and W. E. Dietrich (1995), Field experiments on erosion by overland flow and their implication for a digital terrain model of channel initiation, *Water Resour. Res.*, *31*(11), 2867–2876.

Prosser, I. P., and M. Soufi (1998), Controls on gully formation following forest clearing in a humid temperate environment, *Water Resour. Res.*, *34*(12), 3661–3671.

Prosser, I.P., and L. Williams (1998), The effect of wildfire on runoff and erosion in native Eucalyptus forest, *Hydrol. Processes*, *12*, 251–265.

Ree, W. O., F. L. Wimberley, and F. R. Crow (1977), Manning's n and the overland flow equation, *Trans. Am. Soc. Agric. Eng.*, *20*(1), 89–95.

Reeves, G. H., P. A. Bisson, and J. M. Dambacher (1998), Fish communities, in *River Ecology and Management: Lessons From the Pacific Coastal Ecoregion*, edited by R. J. Naiman and R. E. Bilby, pp. 200–234, Springer-Verlag, New York.

Riebe, C. S., J. W. Kirchner, D. E. Granger, and R. C. Finkel (2001), Minimal climatic control on erosion rates in the Sierra Nevada, California, *Geology*, *29*, 447–450.

Schaake, J. C., V. I. Koren, Q.-Y. Duan, K. Mitchell, and F. Chen (1996), Simple water balance model for estimating runoff at different spatial and temporal scales, *J. Geophys. Res.*, *101*(D3), 7461–7475.

Schmidt, K. M., D. R. Montgomery, S. Schaub, J. J. Roering, J. D. Stock, and W. E. Dietrich (2002), The variability of root cohesion as an influence on shallow landslide susceptibility in the Oregon Coast Range, *Can. Geotech. J.*, *38*(5), 995–1024.

Selby, M. J. (1993), *Hillslope Materials and Processes*, 451 pp., Oxford Univ. Press, New York.

Shakesby, R. A., S. H. Doerr, and R. P. D. Walsh (2000), The erosional impact of soil hydrophobicity: Current problems and future research directions, *J. Hydrol.*, *231–232*, 178–191.

Sidle, R. C. (1991), A conceptual model of changes in root cohesion in response to vegetation management, *J. Environ. Qual.*, *20*, 43–52.

Sidle, R. C. (1992), A theoretical model of the effects of timber harvesting on slope stability, *Water Resour. Res.*, *28*(7), 1897–1910.

Sidle, R. C., A. J. Pearce, and C. L. O'Loughlin (Eds.) (1985), *Hillslope Stability and Land Use*, *Water Resour. Monogr.*, vol. 11, edited by R. C. Sidle et al., 140 pp., AGU, Washington, D. C.

Smith, R. E., D. C. Goodrich, D. A. Woolhiser, and C. L. Unkrich (1995), Kineros— A kinematic runoff and erosion model, in *Computer Models of Watershed Hydrology*, edited by V. P. Singh, pp. 697–732, Water Resour. Publ., Highlands Ranch, Colo.

Stock, J., and W. E. Dietrich (2003), Valley incision by debris flows: Evidence of a topographic signature, *Water Resour. Res.*, *39*(4), 1089, doi:10.1029/2001WR001057.

Tarboton, D. G. (1997), A new method for the determination of flow directions and upslope areas in grid digital elevation models, *Water Resour. Res.*, *33*(2), 309–319.

Tucker, G. E., and R. L. Bras (1998), Hillslope processes, drainage density, and landscape morphology, *Water Resour. Res.*, *34*(10), 2751–2764.

Tucker, G. E., and R. L. Bras (2000), A stochastic approach to modeling the role of rainfall variability in drainage basin evolution, *Water Resour. Res.*, *36*(7), 1953–1964.

Tucker, G. E., and R. Slingerland (1997), Drainage basin responses to climate change, *Water Resour. Res.*, *33*(8), 2031–2047.

U.S. Department of Agriculture Forest Service (1990), Land and resource management plan for the Boise national forest, Ogden, Utah.

Walsh, R. P. D., C. D. O. Coelho, A. Elmes, A. J. D. Ferreira, A. J. B. Goncalves, R. A. Shakesby, J. L. Ternan, and A. G. Williams (1998), Rainfall simulation plot experiments as a tool in overland flow and soil erosion assessment, north central Portugal, *GeoOkoDynamic*, *19*, 139–152.

Welch, E. B., J. M. Jacoby, and C. W. May (1998), Stream quality, in *River Ecology and Management: Lessons From the Pacific Coastal Ecoregion*, edited by R. J. Naiman and R. E. Bilby, pp. 69–94, Springer-Verlag, New York.

Wells, W. G. (1987), The effects of fire on the generation of debris flows in southern California, in *Debris Flows/Avalanches, Process, Recognition, and Mitigation*, edited by J. E. Costa and G. F. Wieczorek, *Rev. Eng. Geol.*, *12*, 105–114.

Willgoose, G., R. L. Bras, and I. Rodriguez-Iturbe (1991), A coupled channel network growth and hillslope evolution model: 1. Theory, *Water Resour. Res.*, *27*(7), 1671–1684.

Wolman, M. G., and J. P. Miller (1960), Magnitude and frequency of forces in geomorphic processes, *J. Geol.*, *68*, 54–74.

Wu, W., and R. C. Sidle (1995), A distributed slope stability model for steep forested basins, *Water Resour. Res.*, *31*(8), 2097–2110.

Yu, B. (1998), Theoretical justification of SCS method for runoff estimation, *J. Irrig. Drain. Eng.*, *124*(6), 306–309.

Ziemer, R. R., and T. E. Lisle (1998), Hydrology, in *River Ecology and Management: Lessons From the Pacific Coastal Ecoregion*, edited by R. J. Naiman and R. E. Bilby, pp. 43–68, Springer-Verlag, New York.

————————————

E. Istanbulluoglu, Department of Civil and Environmental Engineering, Massachusetts Institute of Technology, MIT Room 48-114, Cambridge, MA 02139, USA. (erkan@mit.edu)

C. H. Luce, Rocky Mountain Research Station, U.S. Forest Service, 316 East Myrtle Street, Boise, ID 83702, USA. (cluce@rmci.net)

R. T. Pack and D. G. Tarboton, Civil and Environmental Engineering Department, Utah State University, 8200 Old Main Hill, Logan, UT 84322-4110, USA. (rtpack@cc.usu.edu; dtarb@cc.usu.edu)